Stability of two-layer flows past slippery surfaces. I. Horizontal channels

Cite as: Phys. Fluids **33**, 084112 (2021); https://doi.org/10.1063/5.0050256
Submitted: 13 March 2021 • Accepted: 06 June 2021 • Published Online: 27 August 2021

Vignesh Ramakrishnan, Remil Mushthaq, Anubhab Roy, et al.

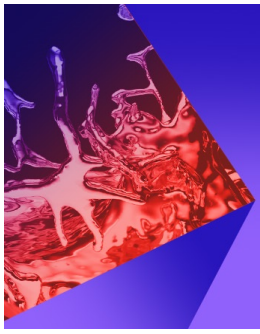

Physics of Fluids ARTICLE scitation.org/journal/phf

Stability of two-layer flows past slippery surfaces. I. Horizontal channels

Cite as: Phys. Fluids 33, 084112 (2021); doi: 10.1063/5.0050256
Submitted: 13 March 2021 · Accepted: 6 June 2021 ·
Published Online: 27 August 2021

Vignesh Ramakrishnan,[1,a] Remil Mushthaq,[1,b] Anubhab Roy,[1,c] and S. Vengadesan[1,2]

AFFILIATIONS

[1]Department of Applied Mechanics, Indian Institute of Technology Madras, Chennai 600036, India
[2]Department of Mechanical Engineering, Virginia Tech, Blacksburg, Virginia 24061, USA

[a]**Present address:** Postgraduate Student, Technische Universität Dresden, Germany.
[b]**Present address:** Department of Mechanical Engineering, University of New Hampshire, Durham, New Hampshire 03824, USA.
[c]**Author to whom correspondence should be addressed:** anubhab@iitm.ac.in

ABSTRACT

We study the role of wall slip on the stability of a two-layered plane Poiseuille flow. The equations of motion for the base flow state are derived, and a linear stability analysis is carried out to arrive at the fourth-order Orr–Sommerfeld equations for the fluid layers. An asymptotic analysis is conducted for wavenumbers in the long wavelength limit. The Orr–Sommerfeld equations are solved numerically using a multidomain Chebyshev Collocation Method to arrive at the spectrum of eigenvalues and their associated eigenfunctions. The effect of wall slip on the stability characteristics of the flow system is examined in greater detail. It is observed that slip brings about a stabilizing, as well as a destabilizing effect on the flow system.

I. INTRODUCTION

This paper presents a study of the hydrodynamic stability of a two-layered plane Poiseuille flow, with the channel walls modeled as slippery surfaces. Two-layered Poiseuille flows are encountered in many industrial applications—flow of gas and condensate in pipelines, gas–liquid flows in chemical reactors, polymer processing, microchannel flows, and coating industries, to name a few. Thus, an instability study of the same and its dependence on different operational parameters are of practical importance.

The stability of two-layered plane Poiseuille flows is a well-researched area in fluid dynamics, and there have been numerous works regarding the same. One of the earliest studies in this area was carried out by Yih,[1] when he studied the stability of a viscosity-stratified channel flow to long wave disturbances. Yih observed that, even at arbitrary low Reynolds numbers, there exists an instability, arising as a result of viscosity stratification. Yih termed this mode of instability as interfacial mode and claimed that this was different from the Tollmein–Schlichtling (shear) mode of instability, which arises at significantly larger Reynolds numbers. Later, Charru and Fabre[4] observed that this instability caused due to viscosity stratification can be stabilized by implementing a density stratification in the flow system, when they conducted a linear stability analysis of a viscosity-stratified Couette–Poiseuille flow.

A stability analysis of an unbounded Couette flow of two fluids having different viscosities and densities, by Hooper and Boyd,[2] revealed that the interface may be unstable to short wave perturbations as well, and that the presence of rigid boundaries does not influence the interfacial mode of instability. Yiantsios and Higgins[3] extended Yih's research to short wavelength disturbances and carried out a numerical analysis, which accounted for effects arising as a result of density stratification, thickness ratio of fluid layers, and gravity and interfacial surface tension. They showed that, at given values of thickness ratios, two-layered channel flows are unstable to more than one mode. The influence of thickness ratios and the mean interfacial height on the flow system was subsequently studied in greater detail by Tilley *et al.*,[5] who performed a stability analysis of air–water flow in horizontal and inclined channels.

A detailed study of the spectral characteristics and eigenfunction structures related to the interfacial and shear modes of instability was conducted by Kaffel and Riaz.[7] The interaction between the two modes and the effect of mode coalescence was discussed. They also observed that, for certain parameter combinations, coalescence may occur in both stable and unstable flow regimes. More recently, Barmak *et al.*[8] conducted a stability study of two-layer plane-parallel flows for liquid–liquid and gas–liquid systems and observed that there is no correlation between the perturbation wavelength and the type of

instability. They also studied the effect of channel height on the stability of gas–liquid flow and observed that, for a channel height smaller than its critical value, the sole disturbances are long wave perturbations. Intermediate/short wave perturbations are the critical disturbances when the channel height is greater than its critical value.

All these studies have prescribed the usage of the no-slip condition at the channel walls, which assumes that the relative velocity at the solid walls goes to zero. While there is considerable experimental proof backing the validity of the no-slip condition for a number of macroscopic flows, some recent experiments conclude that there is a breakdown in the no-slip condition for microscopic flows driven by pressure gradients, and shear or electric fields. The concept of a slip boundary was first proposed by Navier,[9] who came up with a general boundary condition that takes into account the possibility of fluid slip at a solid surface. Navier's boundary condition assumes that fluid velocity u at a solid surface is directly proportional to the shear stress at the surface

$$\mathbf{u} = \mathbf{U} + \frac{\lambda}{\mu}(\boldsymbol{\delta} - \mathbf{nn}).(\boldsymbol{\sigma}.\mathbf{n}), \tag{1}$$

where $\mathbf{U}$ is the velocity of the surface, λ is the slip length, μ is the viscosity of the fluid, $\boldsymbol{\delta}$ represents the identity tensor, $\mathbf{n}$ is the unit normal, and $\boldsymbol{\sigma}$ is the total stress tensor. Slip length is defined as the equivalent local distance below the rigid surface where the no-slip condition can be satisfied if the flow field is extended outside the physical domain. The no-slip condition is obtained when $\lambda = 0$. A finite value of λ corresponds to a fluid slip at the wall. In the case of macroscopic flows, since the length scales involved are significantly larger than the value of slip length λ, it is sufficient to consider the no-slip boundary condition. However, in the case of microscale flows, λ is a finite quantity and plays a significant role in calculation of fluid velocity.

Experimental studies conducted by Watanabe and Mizunuma,[10] Tretheway and Meinhart,[11] Pit *et al.*,[12] Zhu and Granick,[13] and Craig *et al.*[14] observe that the no-slip condition ceases to be accurate in micro- and nano-scale flows, and report slip lengths ranging from 20 nm[14] to as high as 1 μ m.[11,13] Molecular dynamics simulations conducted by Thompson and Troian[15] and Sun and Ebner[16] have also confirmed the existence of velocity slip at solid–liquid interfaces, depending on several interfacial parameters.

A number of studies have also confirmed the occurrence of slip in macro scale flows over hydrophobic surfaces[17,18] and report slip lengths ranging from a few nanometers to a micrometer. Hydrophobic surfaces can be treated chemically by introducing nanoscale extrusions on the surface, such that the contact angle between the fluid droplet and the surface increases beyond 150°. Such surfaces are termed as superhydrophobic surfaces. Several studies have reported that fluid flow over superhydrophobic surfaces tends to produce greater slip lengths, and, thus, aid in drag reduction of the flow. Similar results were obtained by Ichikawa *et al.*,[19] as they conducted an experimental study to estimate the drag reduction effect in hydrophobic microchannel flows. This property of superhydrophobic surfaces has led to their utilization in many industrial applications—self-cleaning surfaces, deicing, and anti-corrosive coatings to name a few. Voronov and Papavassiliou's paper[20] provides an excellent literature review of fluid slip over superhydrophobic surfaces. More recently, Liu and Zhang[21] conducted a study on natural transition locations in flat-plate boundary layers on superhydrophobic surfaces. They concluded that superhydrophobic surfaces bring about a delay in the natural transition and that this delay effect becomes stronger with increase in slip length.

The phenomenon of velocity slip is also prevalent in flows over permeable surfaces and porous media. Beavers and Joseph[22] conducted a macroscopic modeling of transport phenomena at the interface between a fluid and a porous region. They assumed flow in the fluid and porous layers to be governed by the Navier–Stokes equation and the Darcy equation, respectively, and proposed a new slip flow boundary condition at the interface, which was consistent with experimental results.

Several studies of the effect of wall slip on the stability of one- and two-layered channel flows have been previously carried out.[23–29,31–35] Gersting[23] conducted a linear stability analysis of a flow between two parallel plane porous plates with velocity slip boundary condition implemented at the plates, and observed that an increase in slip results in stabilization of the flow, by increasing the value of critical Reynolds numbers of instability. This result was also confirmed by Lauga and Cossu,[24] who conducted a stability analysis on a pressure driven slippery channel flow, where slip was imparted both symmetrically (on both channel walls) and anti-symmetrically (different values of slip length at both walls). Min and Kim[25] conducted a similar study to observe the effect of slip on the stability and transition in wall-bounded shear flows. They observed that the critical Reynolds number increases with streamwise slip, thus delaying the transition to turbulence. However, the introduction of spanwise slip induces an earlier transition. Ling *et al.*[26] further touched upon the study proposed by Lauga and Cossu[24] and Min and Kim,[25] by considering different values of slip at the channel walls (asymmetric slip). They observed that the introduction of slip results in a stabilizing as well as a destabilizing effect, depending on the value of slip length chosen. Chai and Song[27] revisited this study and explored a broader range of slip lengths. They observed that streamwise slip leads to a suppression in the nonmodal transient growth of the system, whereas spanwise slip leads to a subsequent increase in nonmodal transient growth. A further investigation of the effect of slip velocity on the nonmodal transient growth was also conducted by Samanta.[28] Pascal[34] carried out a linear stability analysis of a thin film flow down an inclined porous surface, in the long wavelength limit. The flow through porous media is governed by Darcy's law, and his results showed that increasing the permeability of the inclined porous surface had a destabilizing effect on the flow system. Samanta *et al.*[31] conducted a linear stability analysis of a falling film down a slippery plane and were able to arrive at a similar result as depicted in Pascal's work[34] that the introduction of slip brings about a destabilizing effect on the flow system at the onset of instability. However, they also observed that, at high Reynolds numbers, the implementation of the Navier's slip boundary condition had a stabilizing effect on the flow system. A similar destabilizing effect of velocity slip on long wavelength disturbances was observed by Chakraborty *et al.*,[35] in their stability analysis of a power-law fluid moving down a slippery inclined plane. However, the presence of a slippery substrate brought about a stabilizing effect at moderate to large wavenumbers.

More recently, Chattopadhyay and Usha[29] conducted an instability study of two-phase plane Poiseuille flow in a hydrophobic channel and observed that slip results in increasing the stability of the system for appropriate viscosity, density, and thickness ratios. They considered values of dimensionless slip number to be 0.05.

The current study focuses on stability of a two-layered, horizontal, slippery channel flow by solving the Orr–Sommerfeld system of equations, which are derived from the Navier–Stokes equations, when subjected to infinitesimal perturbations. It aims to extend the investigations carried out by Yiantsios and Higgins[3] on the linear stability of a pressure driven, two-layered channel flow with channel walls modeled to be slippery surfaces, while considering arbitrary wavenumber disturbances and factoring arbitrary values of wall slip. We have also carried out a complementary investigation on the stability of two-layer flow in slippery inclined channels in Paper II. The results of this work can be found in the paper of Mishra *et al.*

The paper is structured as follows: The governing equations and the geometry are given in Sec. II. The equations for the base flow state are provided in Sec. III. The linear stability analysis and the linearized governing equations are given in Sec. IV, and the asymptotic analysis for long wavelength disturbances is provided in Sec. V. The numerical method is presented in Sec. VII, and the stability results are discussed in Sec. VIII.

II. GOVERNING EQUATIONS

We consider the flow of two-dimensional incompressible, immiscible fluids in a horizontal channel, as shown in Fig. 1. The flow is assumed to be isothermal and is driven by an imposed pressure gradient. The governing equations for this flow configuration are the dimensionless continuity and momentum equations as given below:

$$\frac{\partial u_j}{\partial x}+\frac{\partial v_j}{\partial y}=0, \tag{2}$$

$$\frac{\partial u_j}{\partial t}+u_j\frac{\partial u_j}{\partial x}+v_j\frac{\partial u_j}{\partial y}=-\frac{\rho_1}{r\rho_j}\frac{\partial p_j}{\partial x}+\frac{1}{Re_2}\frac{\upsilon_j}{\upsilon_2}\left(\frac{\partial^2 u_j}{\partial x^2}+\frac{\partial^2 u_j}{\partial y^2}\right), \tag{3}$$

$$\frac{\partial v_j}{\partial t}+u_j\frac{\partial v_j}{\partial x}+v_j\frac{\partial v_j}{\partial y}=-\frac{\rho_1}{r\rho_j}\frac{\partial p_j}{\partial y}+\frac{1}{Re_2}\frac{\upsilon_j}{\upsilon_2}\left(\frac{\partial^2 v_j}{\partial x^2}+\frac{\partial^2 v_j}{\partial y^2}\right)-\frac{1}{Fr_2}. \tag{4}$$

Here, (u_j, v_j) are the x and y components of velocity, υ_j the kinematic viscosity, and p_j the pressure in the fluid layer j. The equations are non-dimensionalized taking h_2—the height of the upper layer and U_I—interfacial velocity, as the scales of length and velocity, respectively. Time is scaled by $\frac{h_2}{U_I}$, and pressure is scaled by $\rho_2 U_I^2$. A list of the dimensionless parameters used in the paper, along with their definitions is given in Table I

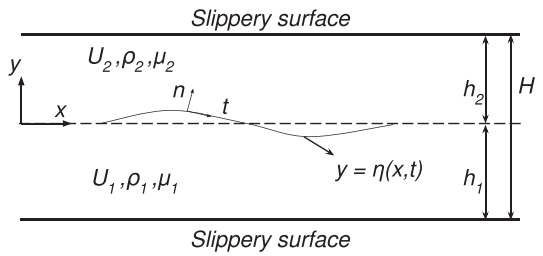

FIG. 1. Schematic of flow configuration. The lower layer is labeled as fluid 1, and the upper layer fluid 2. The two fluids are separated by an interface (located at $y=0$). The interface is assumed to be flat in the base flow case. The total height of the channel is denoted by H, and h_1 and h_2 are the holdups of fluid layers 1 and 2, respectively. ρ_j, μ_j and q_j are the fluid density, dynamic viscosity, and fluid flow rate of fluid layer j, where $j=(1,2)$.

A. Boundary conditions

At the channel walls, these equations are subject to the following boundary conditions:

$$u_1=\beta\frac{\partial u_1}{\partial y} \quad \text{at } y=-n, \tag{5}$$

$$u_2=-\beta\frac{\partial u_2}{\partial y} \quad \text{at } y=1. \tag{6}$$

Here, $\beta=\frac{\lambda}{h_2}$ is the non-dimensionalized slip length, as per Navier slip Condition. A significant number of experimental studies have been conducted to determine an appropriate value of slip length to be considered. Lumma *et al.*[37] had conducted an experimental approach using double-focus fluorescence cross-correlation to determine the value of slip length at the solid interface. They had observed a slip length of 1 μm in a 100 μm channel. This corresponds to a slip length of $\beta=0.01$. Also, Boehnke *et al.*[38] measured the slip length by calculating the sedimentation speed of spherical particles under the influence of gravity. The slip length in this case was observed to be of $O(10^{-1})$. The research paper of Lauga *et al.*[39] provides a comprehensive review of the slip boundary condition and measurement of slip length. Consequently, we have considered a variety of slip lengths ranging from $\beta=0.01$ to $\beta=0.1$ in our study. Earlier, we mentioned that flow over corrugated porous surfaces could be modeled with an effective slip boundary condition. Experiments on boundary layer flow over porous flat plates have shown that the wall slip depends on the porosity, and a characteristic β (non-dimensionalized by displacement thickness) can be >0.1.[40,41] Characterization of slip length via detailed numerical simulations for flows over porous media also correspond to $\beta>0.1$, varying with volume fraction and permeability.[42] The range of β explored in this study is intended to address a diverse spectrum of problems where slip boundary conditions act as a good model, from

TABLE I. Definitions for the dimensionless parameters.

Definition	Dimensionless parameter
$m=\frac{\mu_1}{\mu_2}$	The viscosity ratio of fluid 1 with respect to fluid 2
$n=\frac{h_1}{h_2}$	The ratio of height of fluid layer 1 with respect to height of fluid layer 2
$r=\frac{\rho_1}{\rho_2}$	The ratio of density of fluid 1 with respect to fluid 2
$Re_2=\frac{\rho_2 U_I h_2}{\mu_2}$	Reynolds number of fluid layer 2
$Fr_2=\frac{U_I^2}{gh_2}$	Froude number of fluid layer 2
$We_2=\frac{\rho_2 h_2 U_I^2}{\gamma}$	Weber number of fluid layer 2
γ	Interfacial surface tension coefficient
$\beta=\frac{\lambda}{h_2}$	Slip length

breakdown of continuum approximation to flow past hydrophobic surfaces and adjacent to porous media.

At the interface ($y = 0$), the fluid velocities are equal and tangential stress across the interface is continuous. There is a jump in the normal stress across the interface due to the effect of surface tension. The normal velocity components at the interface satisfy the kinematic boundary condition as given in the following equations:

$$u_1 = u_2, \tag{7}$$

$$v_j = \frac{\partial \eta}{\partial t} + u_j \frac{\partial \eta}{\partial x}, \tag{8}$$

$$[\mathbf{t}\cdot\mathbf{T}\cdot\mathbf{n}] = \left[\frac{m\mu}{\mu_1}\left\{\left(\frac{\partial u}{\partial y}+\frac{\partial v}{\partial x}\right)\left(1-\left(\frac{\partial \eta}{\partial x}\right)^2\right)-4\frac{\partial u}{\partial x}\frac{\partial \eta}{\partial x}\right\}\right] = 0, \tag{9}$$

$$[\mathbf{n}\cdot\mathbf{T}\cdot\mathbf{n}] = \left[p+\frac{m\mu}{\mu_1}\frac{2Re_2^{-1}}{1+\left(\frac{\partial \eta}{\partial x}\right)^2}\left(\frac{\partial u}{\partial x}\left(1-\left(\frac{\partial \eta}{\partial x}\right)^2\right)+\left(\frac{\partial u}{\partial y}+\frac{\partial v}{\partial x}\right)\frac{\partial \eta}{\partial x}\right)\right] = We_2^{-1}\frac{\frac{\partial^2 \eta}{\partial x^2}}{\left(1+\left(\frac{\partial \eta}{\partial x}\right)^2\right)^{3/2}}. \tag{10}$$

III. BASE STATE PROFILE

We assume that fluid velocity $U(y)$ is parallel to the channel walls and varies only with the vertical co-ordinate y. The flow is assumed to be laminar, steady, and fully developed. The interface is assumed to be flat ($\eta = 0$).

The velocity profiles obtained from the solution of the continuity and momentum equations are

$$U_1 = 1 + a_1 y + b_1 y^2, \tag{11}$$

$$U_2 = 1 + a_2 y + b_2 y^2, \tag{12}$$

where

$$a_1 = \frac{m + 2\beta(m-n) - n^2}{m\left[(n+\beta)^2 + \beta(1+\beta)(2n+1) + n(n\beta+1)\right]}, \tag{13}$$

$$b_1 = -\frac{[(n+\beta) + m(1+\beta)]}{m\left[(n+\beta)^2 + \beta(1+\beta)(2n+1) + n(n\beta+1)\right]}, \tag{14}$$

$$a_2 = ma_1, \quad b_2 = mb_1. \tag{15}$$

It is convenient to represent the base flow characteristics of the system in terms of holdup (h) and fluid flow rate (q). We define the following parameters for this purpose:

$$X^2 = \frac{(-dP/dx)_{1s}}{(-dP/dx)_{2s}} = mq,$$
$$q = \frac{q_1}{q_2}.$$

Here, X^2 is the Martinelli parameter and $(-dP/dx)_{js} = 12\mu_j q_j/H^3$ is the corresponding superficial pressure drop for a single phase flow in the channel, where H is the height of the channel, and q_j is the feed flow rate of fluid j.

The velocity profiles of the fluid layers u_1 and u_2 in a fully developed, laminar, steady flow in a horizontal channel with a smooth interface are obtained by integrating the following momentum equations (as given in Ullmann *et al.*[36]):

$$\mu_1 \frac{\partial^2 u_1}{\partial y^2} = \frac{\partial P}{\partial x}, \quad -h \le y < 0, \tag{16}$$

$$\mu_2 \frac{\partial^2 u_2}{\partial y^2} = \frac{\partial P}{\partial x}, \quad 0 \le y < H - h. \tag{17}$$

Here, h is the height of the bottom layer, and $H - h$ is subsequently the height of the top layer. On integration of the equations above, we get the dimensionless velocity profiles

$$\overline{u_1} = \frac{u_1}{U_{1s}} = \frac{6\bar{P}}{mq}(\bar{y}^2 + a\bar{y} + mb), \quad -\bar{h} \le \bar{y} < 0, \tag{18}$$

$$\overline{u_2} = \frac{u_2}{U_{2s}} = 6\bar{P}(\bar{y}^2 + a\bar{y} + mb), \quad 0 \le \bar{y} < 1 - \bar{h}, \tag{19}$$

where

$$a = \frac{\bar{h}(\bar{h}+2\beta) - (\bar{h}-1)m(\bar{h}-2\beta-1)}{(\beta m + \beta + m) - \bar{h}(m-1)}, \tag{20}$$

$$b = \frac{(2\beta+1)((1-\bar{h})\bar{h}+\beta)}{\bar{h}(m-1) - (\beta m + \beta + m)}, \tag{21}$$

$$\bar{P} = \frac{(-dP/dx)}{(-dP/dx)_{2s}}, \quad \bar{y} = \frac{y}{H}, \quad \bar{h} = \frac{h}{H},$$
$$U_{1s} = \frac{q_1}{H}, \quad U_{2s} = \frac{q_2}{H}.$$

Here, $\bar{h}$ is the holdup of the bottom layer. As per mass conservation equations,

$$\int_{-\bar{h}}^{0} \overline{u_1}\, d\bar{y} = 1,$$
$$\int_{0}^{1-\bar{h}} \overline{u_2}\, d\bar{y} = 1. \tag{22}$$

Substituting Eqs. (18) and (19) into (22), we obtain an expression for $\bar{P}$ in terms of $\bar{h}$, m and q,

$$\bar{P} = \bar{h}(4m(-\beta+\bar{h}-1)(3\beta+\bar{h}) - \bar{h}(4\beta+\bar{h})) + 3(\bar{h}-1)mq(-2\beta+\bar{h}-1)(2\beta+\bar{h})/4(\bar{h}-1)^2\bar{h}((\bar{h}-1)m \times(-4\beta+\bar{h}-1)(3\beta+\bar{h}) - \bar{h}(-3\beta+\bar{h}-1)(4\beta+\bar{h})). \tag{23}$$

The interfacial velocity can be written as

$$\frac{U_I}{U_{2s}} = \frac{6(2\beta+1)\bar{P}((\bar{h}-1)\bar{h}-\beta)}{\beta + \bar{h}(-m) + \bar{h} + \beta m + m}. \tag{24}$$

Figure 2(a) displays the velocity profile of a slippery channel horizontal flow for a more viscous bottom layer $m = 3$. As a result of slip, and differences in fluid viscosities and thicknesses, the slip velocities at the top and bottom walls are unequal. The dependence of this parameter $\frac{U_1 \to y=-n}{U_2 \to y=1}$ as a function of m and n is observed in Fig. 2(b). The slip length is taken to be $\beta = 0.05$. We observe that, as long as $m < 1$

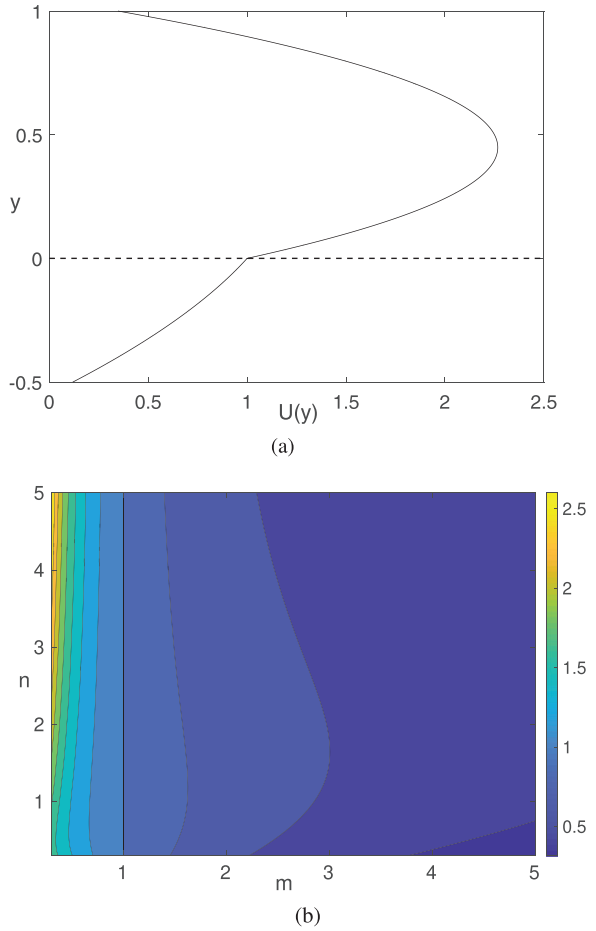

FIG. 2. (a) The velocity profile of a two-layered plane Poiseuille flow is shown. The channel walls are modeled to be slippery surfaces. Flow parameters: $m = 3$, $n = 0.5$, $\beta = 0.05$ (b) Contour plot of the ratio of the velocity slip at the two walls in the plane of viscosity ratio m and thickness ratio n for $\beta = 0.05$.

(viscosity of the upper layer is greater than the lower layer), the slip velocity at the bottom wall is greater than that at the top wall, and vice versa for $m > 1$.

IV. LINEAR STABILITY ANALYSIS

A linear stability analysis of the base flow solution is carried out, with respect to infinitesimal, two-dimensional disturbances. A set of equations, termed as the linear disturbance equations, are derived by splitting the velocity and pressure terms into a mean part and a perturbation part, and substituting them in the governing equations. The perturbed velocities and pressure are denoted as follows:

$$u_j = U_j + u'(x, y, t), \tag{25}$$

$$v_j = v'(x, y, t), \tag{26}$$

$$p_j = P_j + p'(x, y, t). \tag{27}$$

Here, U_j and P_j are the steady state velocity in the x-direction and pressure, respectively.

We then define the disturbance velocities in terms of their corresponding stream functions as

$$u' = \frac{\partial \psi}{\partial y}, \tag{28}$$

$$v' = -\frac{\partial \psi}{\partial x}, \tag{29}$$

where

$$\psi = \phi(y) e^{ik(x-ct)}, \tag{30}$$

$$p' = \hat{P}(y) e^{ik(x-ct)}, \tag{31}$$

$$\eta = H_\eta e^{ik(x-ct)}. \tag{32}$$

The relations for pressure and interfacial perturbation terms are given by Eqs. (31) and (32).

Here, $\hat{P}$ and H_η are the corresponding amplitudes of the pressure and interface perturbation terms, k is the dimensionless wavenumber ($k = 2\pi h_2/l_w$, with l_w being the wavelength), and c is the complex wave speed.

Substituting the relations defined above, into the continuity and momentum equations, we obtain the fourth-order Orr–Sommerfeld equations

$$\phi_j^{iv}(y) - 2k^2\phi_j''(y) + k^4\phi_j = ikRe_2\frac{\nu_2}{\nu_j}\left[(U_j - c)(\phi_j'' - k^2\phi_j) - \phi_j U_j''\right], \quad \text{where } j = 1, 2. \tag{33}$$

The set of boundary conditions to be substituted are as follows:

At the channel walls, due to Navier slip boundary condition

$$\frac{\partial \phi_1}{\partial y} = \beta\frac{\partial^2 \phi_1}{\partial y^2} \quad \text{at } y = -n, \tag{34}$$

$$\frac{\partial \phi_2}{\partial y} = -\beta\frac{\partial^2 \phi_2}{\partial y^2} \quad \text{at } y = 1. \tag{35}$$

At the channel walls due to no penetration condition

$$\phi_2 = 0 \quad \text{at } y = 1, \tag{36}$$

$$\phi_1 = 0 \quad \text{at } y = -n. \tag{37}$$

The interfacial boundary conditions are defined as follows:

$$v' = \frac{\partial \eta}{\partial t} + \frac{\partial \eta}{\partial x}\frac{\partial x}{\partial t} = \frac{D\eta}{Dt} \quad \text{at } y = 0. \tag{38}$$

Substituting (29)–(31) in the above equation and simplifying further, we obtain

$$\phi_1 = H_\eta(c - U_1) \quad \text{at } y = 0, \tag{39}$$

$$\phi_2 = H_\eta(c - U_2) \quad \text{at } y = 0. \tag{40}$$

As a result of the perturbations, the interface is displaced by an amount denoted by η. The fluid velocities at the interface can thus be approximated using a Taylor series expansion

$$u_1(0 + \eta) = u_1(0) + \frac{\partial u_1}{\partial y}(y = 0)\eta, \tag{41}$$

$$u_2(0 + \eta) = u_2(0) + \frac{\partial u_2}{\partial y}(y = 0)\eta. \tag{42}$$

The fluid velocities are equal at the interface, that is, $u_1 = u_2$,

$$\phi_1' + \frac{\phi_1}{c-1}U_1' = \phi_2' + \frac{\phi_2}{c-1}U_2' \quad \text{at } y = 0. \tag{43}$$

Tangential stresses across the interface are equal,

$$\phi_2'' + k^2\phi_2 + U_2''H_\eta = m(\phi_1'' + k^2\phi_1 + U_1''H_\eta) \quad \text{at } y = 0. \tag{44}$$

There is a jump in the normal stress across the interface as a result of the interfacial surface tension

$$\begin{aligned} &m(\phi_1''' - 3k^2\phi_1') - (\phi_2''' - 3k^2\phi_2') \\ &\quad + ik\mathrm{Re}_2\left[r((c-1)\phi_1' + U_1'\phi_1) - ((c-1)\phi_2' + U_2'\phi_2)\right] \\ &= ik\mathrm{Re}_2(\mathscr{F} + k^2\mathscr{S})H_\eta, \end{aligned} \tag{45}$$

where $\mathscr{F} = \frac{(r-1)}{Fr_2}$ is the ratio of the gravitational force to the inertial force, and $\mathscr{S} = \frac{1}{We_2}$ is the ratio of the surface tension force to the inertial force.

Using linear stability analysis, we study the growth of infinitesimal disturbances imposed on the hydrodynamic system. The dimensionless wave speed c is taken to be complex, such that $c = c_R + ic_i$. Here, c_R is the phase speed of the perturbation, and kc_i is the perturbation growth rate. We are particularly interested in the most unstable mode of the disturbance, and for given values of $m, n, r, \beta, F, Re_2, S$, we wish to determine the wave speed c and the associated amplitude of the disturbance ϕ_j.These values are our eigenvalues and their corresponding eigenfunctions. Solving for the values of c, we can determine the reaction of the base state flows depending on the sign of the phase speed c_i. For a positive value of c_i, the perturbations grow with time, and the system is considered to be unstable. Similarly, a negative value of c_i indicates that the system is stable. When $c_i = 0$, the system is neutrally stable.

V. ASYMPTOTIC ANALYSIS

A. Long wave analysis ($k \ll 1$)

A long wave analysis is carried out to study the stability of the hydrodynamic system to perturbations having significantly large wavelengths, in this case, compared to the characteristic length of the problem (width of upper fluid layer, h_2). This can be done by expressing the eigenvalues and eigenfunctions as a regular perturbation series in k,

$$\phi_j = \phi_{j,0} + k\phi_{j,1} + k^2\phi_{j,2} + k^3\phi_{j,3} + \cdots, \tag{46}$$

$$c = c_0 + kc_1 + k^2c_2 + k^3c_3 + \cdots. \tag{47}$$

These expansions are substituted into the Orr–Sommerfeld equations and the boundary conditions, and the terms of like order in "k" are grouped together. The resulting equations in zeroth and first orders of k are solved analytically to obtain expressions for the eigenvalues c_M and the corresponding eigenfunctions ϕ_M (M is the order of the solution).

In the zeroth-order approximation, all terms containing k are omitted from the system of differential equations. In this case, $\phi_j = \phi_{j,0}$, $(j = 1, 2)$ and $c = c_0$. Accordingly, Eq. (46) can be written as

$$\phi_{1,0}^{iv} = 0, \quad \phi_{2,0}^{iv} = 0. \tag{48}$$

The boundary conditions are written below:

$$\phi_{1,0} = 0 \quad \text{at } y = -\mathrm{n}, \tag{49}$$

$$\phi_{2,0} = 0 \quad \text{at } y = 1, \tag{50}$$

$$\phi_{1,0}' = \beta\phi''_{1,0} \quad \text{at } y = -\mathrm{n}, \tag{51}$$

$$\phi_{2,0}' = -\beta\phi''_{2,0} \quad \text{at } y = 1, \tag{52}$$

$$\phi_{1,0}' + \frac{\phi_{1,0}}{c_0 - 1}U_1' = \phi_{2,0}' + \frac{\phi_{2,0}}{c_0 - 1}U_2' \quad \text{at } y = 0, \tag{53}$$

$$\phi''_{2,0} + U''_2\frac{\phi_{2,0}}{c_0 - 1} = m\left(\phi''_{1,0} + U''_1\frac{\phi_{1,0}}{c_0 - 1}\right) \quad \text{at } y = 0, \tag{54}$$

$$m\phi'''_{1,0} - \phi'''_{2,0} = 0 \quad \text{at } y = 0. \tag{55}$$

The solution of (48) is a third-order polynomial given below:

$$\phi_{j,0} = c_0 - 1 + B_{j,0}^1 y + B_{j,0}^2 y^2 + B_{j,0}^3 y^3, \quad j = 1, 2. \tag{56}$$

The constants $B_{1,0}^0$ and $B_{2,0}^0$ are set to $c_0 - 1$ as specified in the analysis conducted by Kushnir *et al.*[6]

An expression for c_0 is obtained by solving Eq. (56). The expressions for the other constants $B_{j,0}^1, B_{j,0}^2, B_{j,0}^3$ are provided in the supplementary material, due to their unwieldy nature:

$$\begin{aligned} c_0 = {} & \beta(m^2(n(n(8n+21)+12)+1) + 2m(n(n+1)(n(2n \\ & + 15) + 17) + 2)n + (n(n(n+12)+21)+8)n^3) \\ & + 4\beta^3(n+1)(m^2(6n+2) + m(n+1)(n(5n+16)+5) \\ & + 2n^2(n+3)) + 2\beta^2(n+1)(m^2(4n(n+4)+3) \\ & + 2m(n(n(n(n+9)+25)+9)+1) + n^2(n(3n+16)+4)) \\ & + n(n+1)(2mn + m + n^2)(m + n(n+2)) \\ & + 24\beta^4 m(n+1)^3/(2\beta + n + 1)(\beta + \beta n + n) \\ & \times ((4\beta+1)m^2 + 2m(6\beta^2(n+1)^2 + 2\beta(n+1)(n(n+5)+1) \\ & + n(n(2n+3)+2)) + n^3(4\beta + n)). \end{aligned} \tag{57}$$

In the first-order approximation, terms containing k^2 and higher order of k are ignored. In this case, $\phi_j = \phi_{j,0} + k\phi_{j,1}(\mathrm{j} = 1, 2)$ and $c = c_0 + kc_1$. Substituting these expressions into Eq. (46), we get

$$\phi_{1,1}^{iv} = iRe_2m^{-1}r\left[(U_1 - c_0)\phi''_{1,0} - \phi_{1,0}U_2''\right], \tag{58}$$

$$\phi_{2,1}^{iv} = iRe_2\left[(U_2 - c_0)\phi''_{2,0} - \phi_{2,0}U_2''\right]. \tag{59}$$

The boundary conditions are written as follows:

$$\phi_{1,1} = 0 \quad \text{at } y = -n, \tag{60}$$

$$\phi_{2,1} = 0 \quad \text{at } y = 1, \tag{61}$$

$$\phi_{1,1}' = \beta\phi''_{1,1} \quad \text{at } y = -n, \tag{62}$$

$$\phi_{2,1}' = -\beta\phi''_{2,1} \quad \text{at } y = 1, \tag{63}$$

$$\phi_{1,1} = \phi_{2,1} \quad \text{at } y = 0, \tag{64}$$

$$\begin{aligned} &c_1\phi_{1,0}' + (c_0 - 1)\phi_{1,1}' + \phi_{1,1}U_1' \\ &\quad = c_1\phi_{2,0}' + (c_0 - 1)\phi_{2,1}' + \phi_{2,1}U_2' \quad \text{at } y = 0, \end{aligned} \tag{65}$$

$$c_1\phi''_{2,0} + (c_0 - 1)\phi''_{2,1} = m(c_1\phi''_{1,0} + (c_0 - 1)\phi''_{1,1}) \quad \text{at } y = 0, \tag{66}$$

$$m\phi'''_{1,1} - \phi'''_{2,1} + iRe_2(r-1)((c_0 - 1)\phi'_{2,0} + U_2'\phi_{2,0}) \tag{67}$$

$$= iRe_2\left(\frac{r-1}{Fr_2} + \frac{k^2}{We_2}\right)\frac{\phi_{2,0}}{(c_0 - 1)} \quad \text{at } y = 0. \tag{68}$$

Here, in spite of eliminating all terms containing k^2 and higher order, we retain a term of $O(k^2)$ in (68) to account for surface tension effects.

The solution of (68) is a third order polynomial given as

$$\phi_{j,1} = iRe_2(B^1_{j,1}y + B^2_{j,1}y^2 + B^3_{j,1}y^3 + \psi_j(y)). \tag{69}$$

The coefficients ($B^1_{j,1}, B^2_{j,1}, B^3_{j,1}$ and ψ_j) mentioned in the above equation are relegated to the supplementary material due to their unwieldy nature.

By solving Eq. (69), we get an expression for c_1,

$$c_1 = \frac{iRe_2 m(c_0 - 1)(B^1_{2,1} - B^1_{1,1})(2\beta + n + 1)(\beta n + \beta + n)}{(m-1)(2\beta m - n(2\beta + n) + m)}. \tag{70}$$

From Eq. (70), we obtain the expression of the complex wave speed to be $c_R = c_0$ and $c_I = -ikc_1$. The flow is stable to long wavelength disturbances when $ic_1 > 0$. In the case of no-slip ($\beta = 0$), it is evident that the denominator goes to zero for $m = 1$ or $m = n^2$. However, we also observe that the terms $c_0 - 1$ as well as $(B^1_{2,1} - B^1_{1,1})$ go to zero when $m = 1$ or $m = n^2$. As a result, Eq. (70) as a whole goes to zero as $m = 1$ or $m = n^2$ for the no-slip case, as is confirmed in the analyses of Yih[1] and Yiantsios and Higgins[3]

In Fig. 3(a), the neutral stability curve is plotted in the plane of viscosity ratio m and thickness ratio n for different values of slip length $\beta = 0, 0.05, 0.1$. Slip is imparted symmetrically on both walls, and long wavelength disturbances are considered ($k = 0.001$). The system is neutrally stable at $m = 1$, that is, when the fluids have the same viscosity, as pointed out by Yih.[1] From the analytical expression for c_1 obtained from our long wavelength calculations [Eq. (70)], it is evident that the flow is neutrally stable for values of $n = \sqrt{m}$ in the no-slip case ($\beta = 0$). This was shown by Yiantsios and Higgins.[3] We notice that the introduction of slip has a destabilizing influence on the flow system, as observed by Samanta *et al.*[35] When the viscosity and thickness of the lower layer are greater than the upper layer ($m > 1, n > 1$), the neutral stability curve is shifted to the right, resulting in an increase in the unstable regions of flow. Similarly, when the viscosity and thickness ratio of the upper layer are greater than that of the lower layer ($m < 1, n < 1$), we observe a destabilizing effect indicated by the leftward shift of the neutral stability curve. The destabilizing role of slip can be seen if we perturb the neutral stability curves for small values of slip. The growth rate in the vicinity of $m = n^2$ curve is

$$\frac{k\,c_I}{Re_2} \sim \frac{(n-1)(m-n^2)}{60n^2(n+1)} + \frac{(n-1)^2}{30n(n+1)}\beta. \tag{71}$$

Thus, in the neighborhood of the $m = n^2$, curve slip always has a destabilizing role as can be seen from Fig. 3(a). The above long wave asymptotic behavior allows us to predict a critical slip that would destabilize an otherwise stable two-layer channel flow in the no-slip case ($m > n^2, n < 1$ and $m < n^2, n > 1$),

$$\beta^{\text{long}}_{\text{critical}} = \frac{|m - n^2|}{2n|n-1|}. \tag{72}$$

As was discussed earlier, $m = 1$ continues to remain a neutral stability curve in the presence of slip. To probe the stability in the vicinity of

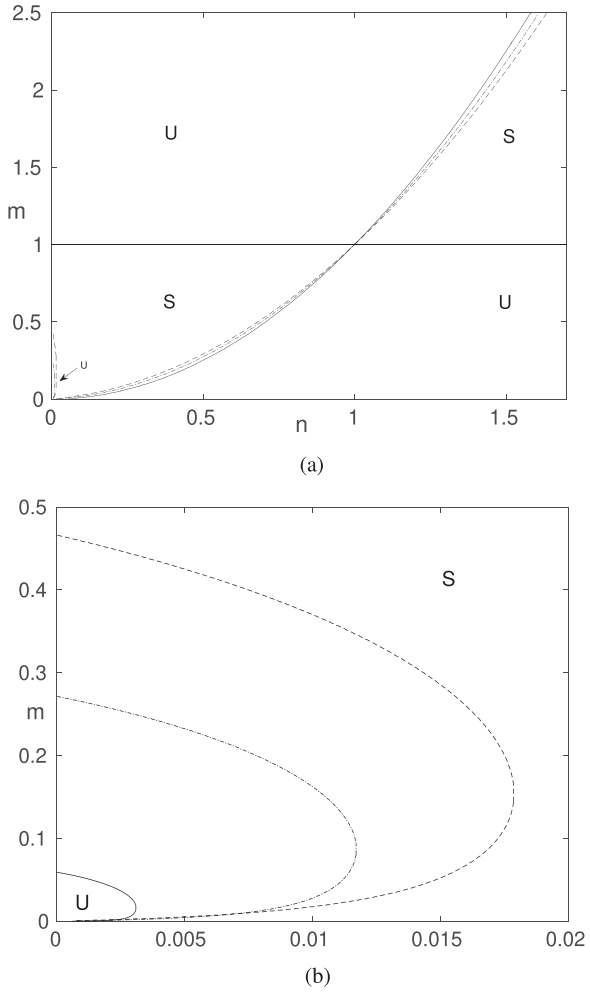

FIG. 3. (a) Neutral stability curve for long wavelength disturbances plotted in the plane of viscosity ratio m and thickness ratio n. (b) A closer view of the influence of slip in regions with small viscosity and thickness ratios. Flow parameters: $r = 1$, $Re_2 = 100$, $\mathscr{F} = \mathscr{S} = 0$ The stable regions are denoted by S, unstable regions by U (a) (—)$\beta = 0$; (·····)$\beta = 0.05$; (- - -) $\beta = 0.1$ (b) (—)$\beta = 0.02$; (·····) $\beta = 0.05$; (- - -)$\beta = 0.1$.

$m = 1$ curve, we consider the following asymptotic expression for the growth rate:

$$\frac{k\,c_I}{Re_2} \sim \frac{(m-1)(1-n)}{420(1+n)^3}(\mathscr{A}_0 - \mathscr{A}_1\beta), \tag{73}$$

where

$$\mathscr{A}_0 = n^4 - 6n^3 + 38n^2 - 6n + 1, \tag{74}$$

$$\mathscr{A}_1 = 4(2n^4 - 23n^3 + 28n^2 - 23n + 2)/(n+1). \tag{75}$$

It can be shown that $\mathscr{A}_0$ is always positive, while $\mathscr{A}_1 < 0$ for $0.0976 < n < 10.242$. Thus, in this range of n, an unstable (stable) mode will be further destabilized (stabilized) by slip. One could argue for slip switching the nature of stability for $n < 0.0976$ or $n > 10.242$

when $m \sim 1$. The critical slip parameter for such a scenario would be $\beta > 0.5$ rendering equation (73) invalid and more importantly the parameter space unphysical. From Fig. 3(b), we also observe that, at very small values of thickness and viscosity ratios, an unstable region of instability emerges with introduction of slip and grows bigger with its subsequent increase. Thus, the present asymptotic analysis should convince the reader that slip has the capacity to both stabilize and destabilize a two-layer channel flow unlike the purely stabilizing role it plays in its single layer counterpart; stemming from the presence of a new interfacial mode and its modification by the weakened flows near the slippery walls.

The growth rate of the interfacial mode is plotted with the viscosity ratio m for different values of thickness ratios n in Fig. 4. Long wavelength disturbances are considered ($k = 0.001$), and the fluids have identical densities ($r = 1$). The other parameters are $Re_2 = 100$ and $\mathscr{S} = 0.1$. Slip lengths of $\beta = 0$, 0.05, and 0.1 are incorporated, and the effect of increasing slip length is observed. The results for the no-slip case are matched with those obtained by Yiantsios and Higgins.[3] For $\beta = 0.05$, the results obtained by the long wave analysis are found to be in agreement with the symmetric slip case studied by Chattopadhyay and Usha.[29] The flow is unstable to long wavelength perturbations when c_1/iRe_2 is positive. When the fluid viscosities are equal, it is observed that the flow becomes neutrally stable, as predicted by Yih.[1] We also observe that the complex wave speed goes to zero at $n = \sqrt{m}$, as shown in the analysis conducted by Yiantsios and Higgins.[3] From the graphs, it is evident that, as the value of slip length β is increased, the stable region displays a decrease. This highlights the destabilizing role played by wall slip.

Figure 5 shows plots of stability maps in the plane of superficial fluid velocities U_{1s} and U_{2s}. Figure 5(a) displays a case wherein the viscosity of the lower fluid is greater than the viscosity of the upper fluid ($m > 1$), with the fluid density being slightly greater than 1, such that the lower fluid is denser than the upper fluid. The channel height is taken to be $H = 0.02$ m. As slip is introduced in the system, we observe that there is an increase in the stable region of flow with increase in slip. We also notice that the critical flow rate q_{cr} decreases with increase in slip. The grayed lines represent lines of constant critical flow rate ratios, which are independent of the densities of the fluids chosen. We observe that there is a decrease in the value of q_{cr} with increase in slip, indicating the stabilizing influence of slip, when the fluid densities are equal ($r = 1$).

In the case of a flow configuration with a more viscous upper layer ($m < 1$), we observe that slip has a destabilizing effect on the stability of the flow system, as shown in Fig. 5(b). We also observe that, as slip is increased upto a value of $\beta = 0.05$, the value of q_{cr} increases, thus indicating an increase in the stable regions of flow when the fluid densities are equal ($r = 1$). Increasing slip beyond this value leads to a decrease in the value of q_{cr}, thus bringing about a destabilizing effect.

Figure 5(c) displays the effect of slip on a flow configuration with high density and viscosity ratios ($m = 55, r = 1000$). We observe an increase in the stable regions of flow with increase in slip. We also observe that the value of q_{cr} increases with increase in slip, thus highlighting the stable influence of slip on a flow configuration with both fluids having the same densities.

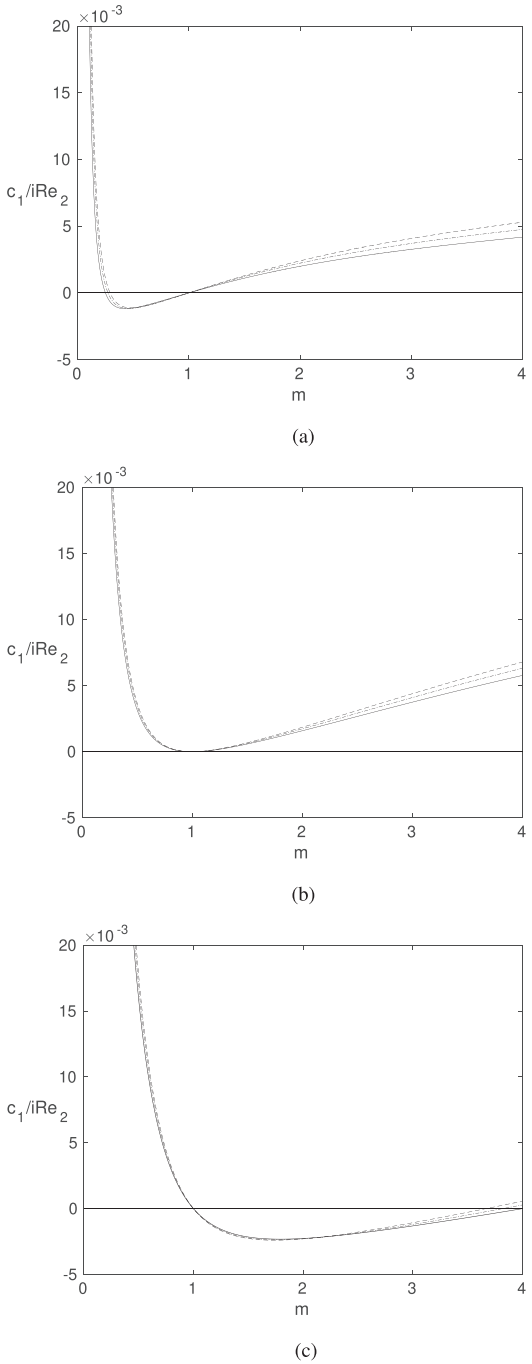

FIG. 4. Dependence of the imaginary part of the wave speed c_1/iRe_2 on m for (a) $n = 0.5$, (b) $n = 1$, (c) $n = 2$. Flow parameters: $Re_2 = 100, r = 1$, $k = 0.001, \mathscr{S} = 0.1$ (—)$\beta = 0$; (·····)$\beta = 0.05$; (- - -) $\beta = 0.1$.

B. Short wave analysis ($k \gg 1$)

A short wave expansion can be carried out by considering the limit $k \gg 1$. We have carried out a short wave analysis in a two-layer channel flow past slippery surfaces. The analysis follows Hooper and

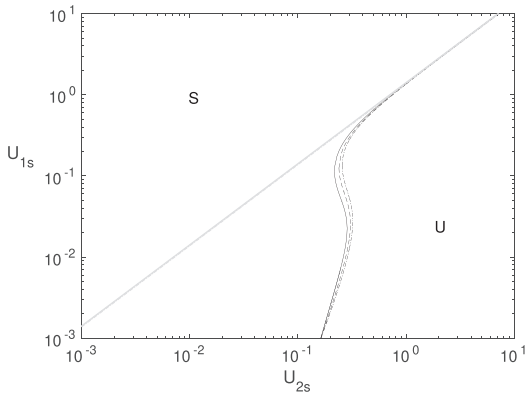

(a)

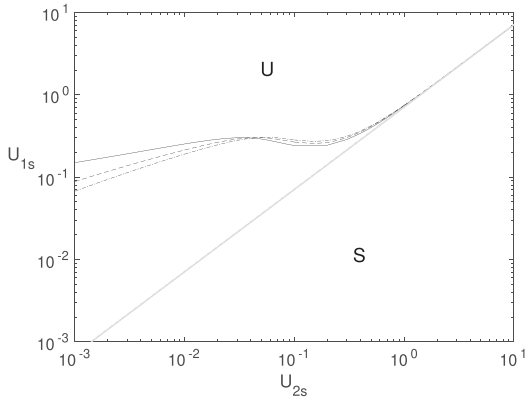

(b)

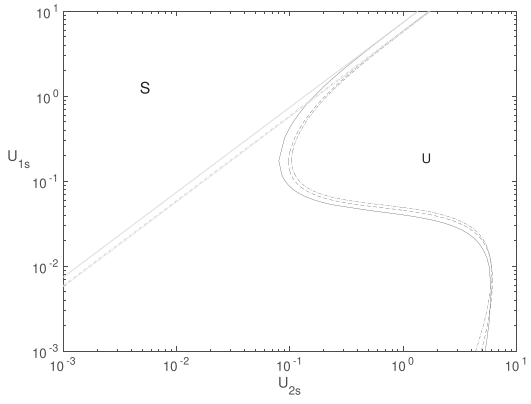

(c)

FIG. 5. Long wave neutral stability curves when (a) $m = 2$, $r = 1.25$, $H = 0.02$ m (b) $m = 0.5$, $r = 1.25$, $H = 0.02$ m (c) $m = 55$, $r = 1000$, $H = 0.02$ m (——)$\beta = 0$; (- - - -)$\beta = 0.05$; (·····)$\beta = 0.1$. Gray lines represent constant values of q_{cr}.

Boyd[2] and Yiantsios and Higgins[3] closely. We define a scaled vertical coordinate

$$Y = ky \tag{76}$$

and pose an asymptotic expansion of the form

$$\phi_j = \phi^*_{j,0}(Y) + k^{-1}\phi^*_{j,1}(Y) + k^{-2}\phi^*_{j,2}(Y) + k^{-3}\phi^*_{j,3}(Y) + \cdots, \tag{77}$$

$$c = c^*_0 + k^{-1}c^*_1 + k^{-2}c^*_2 + k^{-3}c^*_3 = \cdots. \tag{78}$$

If we ignore the effects of gravity and surface tension, we arrive at the following simple expression for the complex wave speed:

$$c = 1 + iRe_2 a_1^2 \frac{(m-1)(m^2-r)}{2(1+m)^2}k^{-3} + O(k^{-4}). \tag{79}$$

The above expression is identical in form to that derived by Yiantsios and Higgins with the effect of slip appearing implicitly via the base state parameter a_1. This is not surprising as in the asymptotic limit of $k \to \infty$, the slippery wall boundary conditions are now applied at $\pm\infty$. Equation (79) shows that short waves are unstable if $m > 1$ and $m > \sqrt{r}$ or $m < 1$ and $m < \sqrt{r}$. We have another neutral stability boundary corresponding to $a_1 = 0$ implying from Eq. (13),

$$m = \frac{n(n+2\beta)}{1+2\beta}. \tag{80}$$

Thus, similar to our long wave calculations, slip destabilizes the short wave instability by shrinking (expanding) the stable (unstable region). We can once again obtain a prediction for the critical slip parameter, a value of β that would destabilize a short wave mode,

$$\beta^{\text{short}}_{\text{critical}} = \frac{|m-n^2|}{4n|n-1|}. \tag{81}$$

VI. NUMERICAL ANALYSIS

It is necessary to solve the eigenvalue problem governed by the Orr–Sommerfeld equations numerically to understand the response of the system to arbitrary wave number disturbances. We use the Chebyshev Collocation method to discretize and solve the Orr–Sommerfeld system of equations. The Chebyshev Collocation method is suitable for problems with non-periodic, bounded domains and has been used extensively in previous research[6–8] for the same purpose.

In order to convert the Orr–Sommerfeld system of equations, defined in the interval $[-n, 1]$ to the Chebyshev Polynomials, defined in the interval $[-1, 1]$, we use an appropriate linear transformation

$$z = \frac{2y+n}{n}, \quad -\text{n} < \text{y} < 0, \tag{82}$$

$$z = 2y - 1, \quad 0 < \text{y} < 1. \tag{83}$$

The eigenfunctions $\phi_j(x)$ are given by the following expansion of the Chebyshev polynomials:

$$\phi_1^{(i)}(z) = \sum_{k=0}^{N_1} a_k T_k^{(i)}(z), \tag{84}$$

$$\phi_2^{(i)}(z) = \sum_{k=0}^{N_2} b_k T_k^{(i)}(z). \tag{85}$$

Here, i denotes the ith derivative with respect to z, $T_k(z)$ represents the Chebyshev polynomials, and a_k and b_k are the discrete Chebyshev expansion coefficients.[30]

The Chebyshev polynomials are interpolated over a set of unevenly spaced grid points, given by

$$z_j = \cos\left(\frac{\pi j}{N}\right). \tag{86}$$

The usage of these points avoid certain errors like the Runge's phenomenon, wherein the errors increase exponentially as $N \to \infty$.

Equations (84) and (85) can be differentiated to obtain the derivatives, which in turn can be substituted into the Orr–Sommerfeld system of equations and boundary conditions to obtain a generalized eigenvalue problem of the form

$$Ax = cBx. \tag{87}$$

This eigenvalue problem was solved in MATLAB®, using the QZ algorithm. By substituting the boundary conditions in rows A and B, we obtain an eigenvalue column vector of dimensions $N_1 + N_2 + 3$. Due to the presence of empty rows in matrix B, some values in the eigenvalue matrix are singular.

VII. RESULTS AND DISCUSSION

In this section, we present the stability behavior of two-layered flows in a horizontal channel. Before carrying out study, we first validated the results obtained from our numerical calculations with the symptotic calculations of Kushnir *et al.*,[6] as well as the numerical results of Yiantsios and Higgins,[3] and the comparisons are presented in Tables II and III. The numerical values of the complex wave speed of the least stable modes in the no-slip case predicted by our numerical code are very much in agreement with those predicted by Yiantsios and Higgins.[3] In Fig. 6, the imaginary part of the eigenvalue is scaled by the value of c_i obtained from the long wavelength analysis [Eq. (70)] and is plotted against kRe_2 for different values of slip length β. We notice that, for small values of kRe_2, there is a good correlation between the values obtained analytically, and the numerical results.

Figure 7 shows a portion of discrete eigenvalues for a non-zero wavenumber ($k = 1$), in the (c_r, c_i) plane. In the absence of viscosity effects ($m = 1$), we obtain the classical Y-shaped eigenspectrum. Three distinct branches of eigenvalues are obtained. The set of eigenvalues toward the left of the spectrum, with the values of c_r going close to zero, is the shear modes of instability. The set of eigenvalues, whose values of c_r tend toward one, are identified as the interfacial modes of instability. A more detailed analysis of the various structures associated with the two modes of instability is presented in the work of Kaffel and Riaz.[7] The eigenspectrum is plotted by taking different values of slip into account ($\beta = 0, 0.05, 0.1$). It is evident that the most unstable shear mode, which takes the value of $c = 0.2345 + 0.003\,397i$ in the no-slip case, becomes stable upon the introduction of slip. As the value of slip length increases, the imaginary part of the eigenvalue decreases. For $\beta = 0.1$, the most unstable shear mode is $c = 0.3351 - 0.016\,01i$. This confirms that slip has a stabilizing effect on high Reynolds

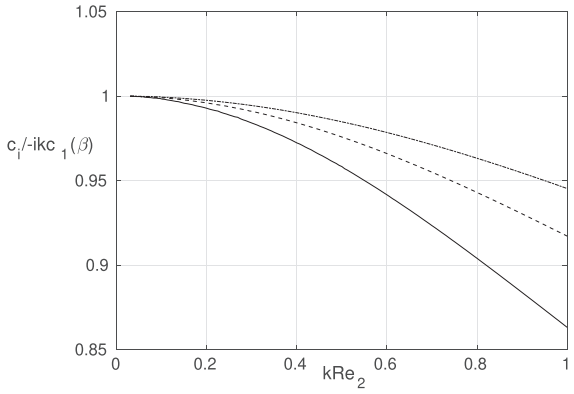

FIG. 6. A plot of imaginary part of the wave speed c_i scaled by c_1 obtained from the long wavelength analysis, as a function of kRe_2 Flow parameters: $m = 30$, $r = 100$, $n = 0.1$, $Re_2 = 5000$, $\mathscr{S} = 0.0125$, $\mathscr{F} = 0.0763$; (——)$\beta = 0$; (- - - - -) $\beta = 0.05$; (·····)$\beta = 0.1$.

TABLE II. Comparison between the present asymptotic and numerical solutions, and Kushnir *et al.*[6] asymptotic results, for $m = 100, r = 2, \mathscr{S} = \frac{25\,000}{(1+n)Re_2^2}, k = \frac{0.001}{(1+n)}$.

n	Re_2	Fr_2	Asymptotic solution (Kushnir *et al.*)[6]	Analytical results [Eq. (70)]	Numerical results (present work)
1/2	4.3269	0.025 275	0.253 063 45 + 0.000 126 022 92i	0.253 063 65 + 0.000 126 023 14i	0.253 063 45 + 0.000 126 567 79i
1/2	4.3269	0.002 527	0.253 063 45 + 0.000 072 337 34i	0.253 063 63 + 0.000 072 326 22i	0.253 063 63 + 0.000 072 959 63i
3	26.2	17.5727	6.218 727 + 0.001 810 625i	6.218 746 + 0.001 810 636i	6.218 751 + 0.001 810 644i
3	26.2	1.757 27	6.218 727 + 0.001 573 444i	6.218 746 + 0.001 573 453i	6.218 751 + 0.001 573 463i

TABLE III. Comparison of the complex wave speed with Yiantsios and Higgins' analysis[3] (m = 5, n = 1, r = 1).

k	Re_2	kS	Numerical results-Yiantsios and Higgins[3]	Numerical results (present work)
10	1	1	0.999 98–0.008 199i	0.999 982–0.008 199i
10	5	1	0.999 56–0.041 184i	0.999 561–0.041 184i
10	1	2	0.999 96–0.016 537i	0.999 964–0.016 537i
10	5	2	0.999 07–0.083 491i	0.999 073–0.083 491i
20	1	1	0.999 997–0.004 145i	0.999 997–0.004 145i
20	5	1	0.999 929–0.020 75i	0.999 929–0.020 75i
20	1	2	0.999 994–0.008 312i	0.999 994–0.008 312i
20	5	2	0.999 855–0.041 664i	0.999 855–0.041 664i

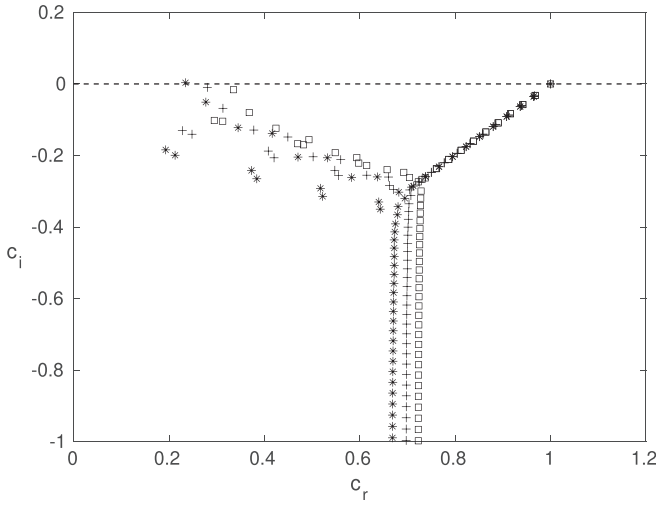

FIG. 7. Eigenspectrum for plane Poiseuille flow. Flow parameters: $n = 1$, $m = 1$, $\mathscr{F} = \mathscr{S} = 0$, $r = 1$, $Re_2 = 10\,000$ (*)—$\beta = 0$; (+)—$\beta = 0.05$; (□)—$\beta = 0.1$.

number flows in the absence of viscosity differences between the phases, gravity effects, and surface tension.

In Figs. 8(a) and 8(b), we plot the neutral stability curve for the interfacial and the shear mode, respectively, in the plane of Reynolds number Re_2 and wavenumber k. We choose to neglect the effect of gravity and interfacial surface tension ($\mathscr{F} = \mathscr{S} = 0$), and the fluid layers are of equal densities ($r = 1$). We observe a stabilizing influence of slip on both the interfacial and shear modes. In Fig. 8(a), it is observed that the interfacial mode is unstable to disturbances of all wavelengths, beyond a particular value of critical Reynolds number. Here, we notice that the value of critical Reynolds number increases from $Re_{cr} = 21$ in the no-slip case, to $Re_{cr} = 24$, when a slip length $\beta = 0.1$ is introduced. With increase in β, the region of stability displays a growth. In Fig. 8(b), we obtain the well-known neutral stability curve for plane Poiseuille flow. Upon introduction of slip, it is observed that neutral stability curve gets shifted toward larger values of Reynolds number, thus indicating a decrease in the unstable region of flow. Here, the critical Reynolds number Re_{cr} increases from 2800 in the no-slip case to 4000, when a slip length $\beta = 0.02$ is introduced. The relation between slip length β and critical Reynolds number is better exemplified in Fig. 9. Our results are in agreement with the analysis of Lauga and Cossu,[24] who carried out a stability analysis of a plane Poiseuille flow in a slippery channel.

Figures 9(a) and 9(b) display a plot of the critical Reynolds number with slip length, for the interfacial and shear mode, respectively, in the absence of gravity and surface tension effects. We notice that, for both interfacial and shear nodes, the critical value of Reynolds number increases with increase in slip length. Here, slip brings about a stabilizing effect in the system, by delaying the transition to instability.

When the viscosity and thickness ratios are taken such that the point (m, n) is located close to the neutral stability curve, as shown in Fig. 3(a), we observe that the introduction of slip has a completely reversible effect on the stability of the fluid system, as shown in Figs. 10(a)–10(d). Here, the most unstable mode of the system c_i decreases in magnitude with increase in slip, upto a critical value of slip length

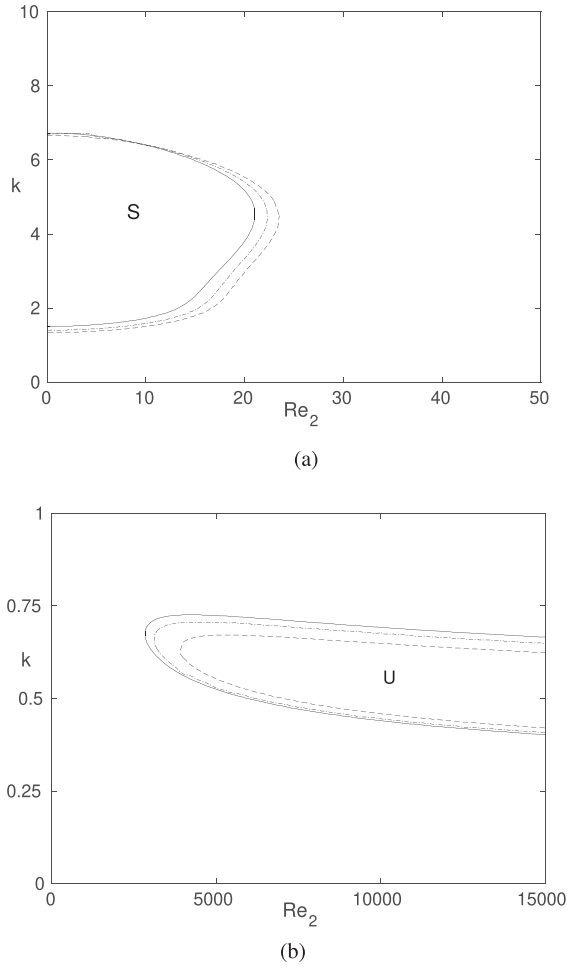

FIG. 8. Neutral stability diagram in the plane of Reynolds number Re and wavenumber k for (a) interfacial mode (—) $\beta = 0$; (- - -) $\beta = 0.05$; (·····) $\beta = 0.1$ (b) shear mode (—) $\beta = 0$; (- - -) $\beta = 0.01$; (·····) $\beta = 0.02$. Flow parameters: $m = 0.75$, $n = 2$, $\mathscr{F} = \mathscr{S} = 0$, $r = 1$ Stable regions are denoted by "S," unstable regions by "U."

($\beta = 0.02$). This is illustrated in Figs. 10(a) and 10(b). When the value of slip length is increased beyond this value, the regions of stability are reversed—the fluid region which was previously stable, becomes unstable, and vice versa. We also notice that a subsequent increase in the slip length beyond this critical value increases the magnitude of the most unstable mode c_i, that is, it destabilizes the flow in the unstable region and brings about a stabilization of the flow in the stable region. This phenomenon is illustrated more clearly in Figs. 10(c) and 10(d).

A similar investigation is made, now considering a slightly different value of viscosity ratio $m = 2.3$, such that the chosen parameters lie on the left of the neutral stability curve for the no-slip case, shown in Fig. 3. All the other parameters are the same as in Fig. 10(a). The slip length varies from $\beta = 0$ to $\beta = 0.1$, and the contour plots of the results obtained are shown in Figs. 11(a)–11(d). We notice that the magnitude of the most unstable mode of the system c_i increases with increase in slip length. Thus, slip brings about a stabilization in the

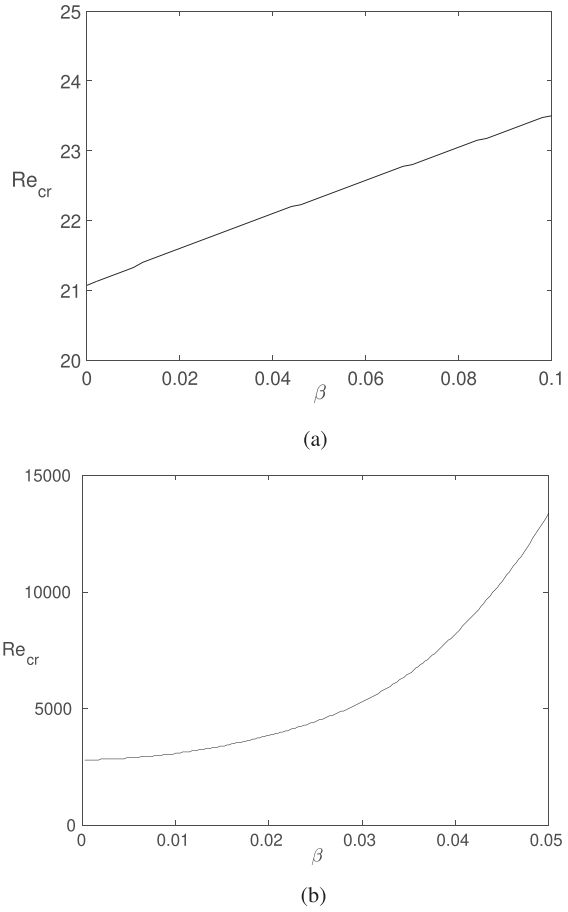

FIG. 9. A plot of critical Reynolds number for linear stability as a function of slip length β for (a) interfacial mode and (b) shear mode Flow parameters are same as in Fig. 8.

stable regions of flow and a subsequent destabilization in the unstable regions of flow. However, there is no change in the regions of stability upon introduction of slip, for the chosen values of β. We also note that, for our chosen value of viscosity ratio, there is no reversal in the regions of stability, which was previously observed in Fig. 10(a).

In Fig. 12, the neutral stability diagram is plotted in the plane of wavenumber k and thickness ratio n for the interfacial mode. The two layers are chosen to have the same densities ($r = 1$), and the effects of gravity and interfacial surface tension are ignored ($\mathscr{F} = \mathscr{S} = 0$). The lower layer is taken to be very viscous when compared to the upper layer ($m = 20$). The curve plotted by the solid lines is presented in the analysis conducted by Yiantsios and Higgins.[3] They highlighted the existence of a straight line at a constant thickness ratio, occurring at $n = \sqrt{m}$. The flow is neutrally stable along this line for all values of k. Upon introduction of slip ($\beta = 0.1$), we observed that the straight line corresponding to neutral stability is shifted to the right, resulting in a stabilizing effect for values of ($k > 0.7$), and a destabilizing effect for values below that.

When the fluid densities are unequal, gravity effects come into play. Yiantsios and Higgins[3] showed that, in the case of a stabilizing density stratification ($F > 0, r > 1$), an increase in the Froude number results in the increase in growth of stable regions of flow, at the expense of the unstable regions. The introduction of slip has a stabilizing, as well as a destabilizing effect on a density stratified flow system. Figure 13 shows a neutral stability diagram with density ratio $r = 1.5$, and $\mathscr{F} = 0.1$, with the value of slip length taken to be $\beta = 0.1$. The curve plotted by the solid lines was depicted in the analysis of Yiantsios and Higgins.[3] The other parameters are the same as those used in Fig. 12. We observe that, as the slip length β is increased, the unstable region of instability at high values of density ratio n decreases. However, the unstable regions of instability for disturbances of wavenumbers $k < 1$ increase slightly with increase in β. This is shown by a shift in the neutral stability curve toward the right.

When slip is introduced to a destabilizing density stratified flow ($F < 0, r < 1$), it results in further destabilization of the flow system. This is displayed in Fig. 14, where a neutral stability curve is plotted with values $\mathscr{F} = -0.01, r = 0.5$, and the other parameters are the same as in Fig. 12. We observe that the stable region of flow at high thickness ratios is reduced upon introduction of slip ($\beta = 0.1$).

Figure 15(a) shows a plot of the neutral stability curve in the plane of wavenumber k and thickness ratio n, for a flow system with equal densities ($r = 1$) and a more viscous upper layer ($m = 0.05$). The Reynolds number is taken to be 1 ($Re_2 = 1$), and the effects of gravity and interfacial surface tension are ignored ($\mathscr{F} = 0, \mathscr{S} = 0$). It is observed that slip brings about a destabilizing effect in the flow system. An increase in the value of slip length β leads to an overall decrease in the stable regions of flow, to the right of the neutral stability line given by $n = \sqrt{m}$. We also observe that this line of neutral stability gets shifted to the left as β increases. As the Reynolds number is increased, there is a drop in the region of stability, as was observed by Yiantsios and Higgins.[3] Figure 15(b) shows the effect of slip on the flow system, taking Reynolds number Re_2 to be 10. Similar to the previous case, we observe a decrease in the stable regions of flow.

When the effect of interfacial surface tension is introduced to the flow system characterized by the set of parameters used in Fig. 12, it brings about a stabilizing effect. The solid curves in Figs. 16(a) and 16(b) represent the neutral stability curves for values of surface tension parameter $\mathscr{S} = 0.01$ and $\mathscr{S} = 10$. It is observed that there is a break in the straight line given by $n = \sqrt{m}$, and a marked increase in regions of stability is seen as the surface tension effect is increased. This was reported in the analysis of Yiantsios and Higgins.[3] The dashed curve indicates the neutral stability curve generated at $\beta = 0.1$. Wall slip plays a destabilizing role in the flow system, as indicated by a rightward shift of the neutral stability curves, thus increasing the unstable region of flow at the expense of the stable regions. However, for large values of thickness ratios, there is a decrease in the unstable regions of flow at high wavenumbers, signifying a stabilizing effect of slip for these parameter ranges.

It is interesting to observe the effect of wall slip on a stabilizing gravity-stratified flow system ($\mathscr{F} > 0, r > 1$), when the viscosity of the upper layer is significantly higher than the lower layer ($m = 0.05$). This is displayed in Figs. 17(a)–17(d). A similar series of plots were shown in Yiantsios and Higgins' paper[3] for the no-slip case. The plots shown are for different values of Froude number $\mathscr{F}$, ranging from $\mathscr{F} = 0.5$ to $\mathscr{F} = 2$. The dotted lines represent the neutral stability curves for $\beta = 0.1$.

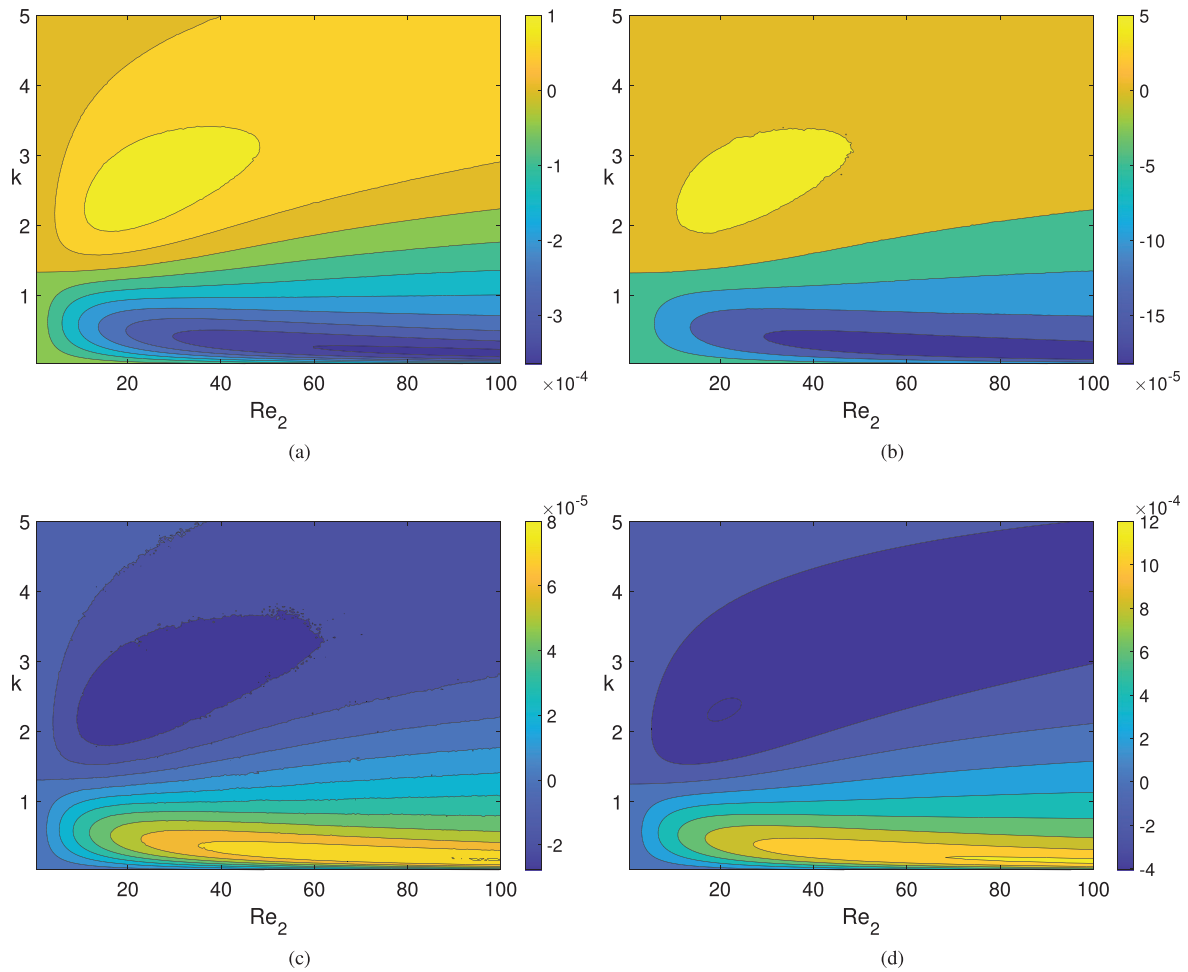

FIG. 10. Contour plot of the most unstable mode c_i in the plane of Reynolds number Re_2 and wavenumber k for the interfacial mode Flow parameters: $m = 2.25$, $n = 1.51$, $\mathscr{F} = \mathscr{S} = 0$, $r = 1$ (a) $\beta = 0$, (b) $\beta = 0.01$, (c) $\beta = 0.025$, (d) $\beta = 0.1$. The color bar represents the value of c_i—the most unstable mode of the system.

It is observed that the introduction of slip has a stabilizing as well as destabilizing effect on the flow system, depending on the set of parameters used. We observe that the introduction of slip stabilizes certain unstable regions of flow, as observed when the unstable region of flow at low wavenumbers and thickness ratios in figure (c), and the regions of flow at high wavenumbers and thickness ratios in (b), (c), and (d) are reduced. Slip also brings about a destabilizing effect at high thickness ratios. It is known that increasing the value of $\mathscr{F}$ brings about a stabilizing influence in the system. Incorporating wall slip in the case destabilizes almost the entirety of the system, with the exception being at large wavenumbers.

VIII. SUMMARY AND CONCLUSIONS

In this study, the stability characteristics of a plane Poiseuille flow with slippery channel walls are studied. The equations of motion for the base flow state are derived, and a linear stability analysis is carried out to arrive at the 4th-order Orr–Sommerfeld equations for the fluid layers. An asymptotic analysis is conducted for wavenumbers in the long wavelength limit. The Orr–Sommerfeld equations are solved numerically using a multi-domain Chebyshev Collocation spectral method. The solutions obtained from numerical simulations are validated with the asymptotic results in the long wavelength limit.

We observe that the introduction of slip plays a dual role in the stability of a flow system—it brings about both stabilizing and destabilizing effects, depending on the flow parameters chosen and the value of slip length β taken. When the lower layer is more viscous than the upper layer ($m > 1$), an introduction of slip leads to a destabilization of the flow system, as a result of an increase in the unstable regions of flow at the expense of the stable regions. When the upper layer is the more viscous of the two ($m < 1$), we observe the emergence of new stable regions of flow upon introduction of slip. We also observe the emergence of an unstable region of flow, when the lower layer is significantly smaller than the upper layer ($n < 0.01$).

It is also observed that the critical value of Reynolds number for instability (Re_{cr}) increases with increase in slip length for both the

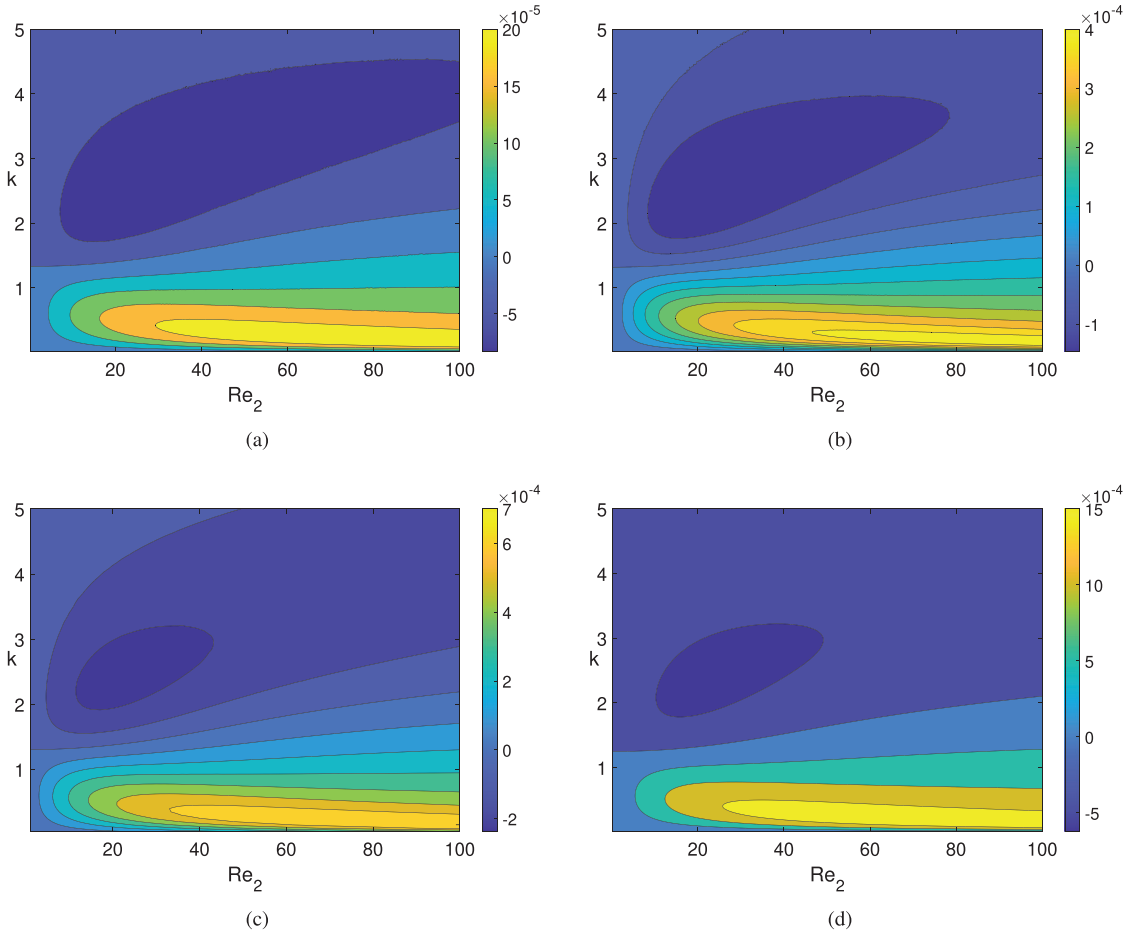

FIG. 11. Contour plot of the most unstable mode c_i in the plane of Reynolds number Re_2 and wavenumber k for the interfacial mode Flow parameters: $m = 2.3$, $n = 1.51$, $\mathscr{F} = \mathscr{S} = 0$, $r = 1$ (a) $\beta = 0$, (b) $\beta = 0.01$, (c) $\beta = 0.025$, (d) $\beta = 0.1$.

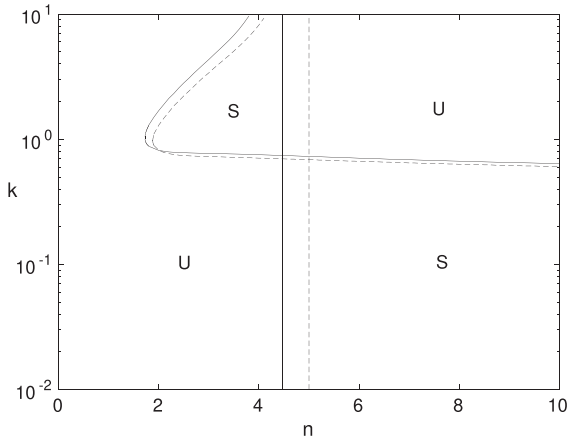

FIG. 12. Neutral stability diagram plotted in the plane of wave number k and thickness ratio n for the interfacial mode. Flow parameters: $Re_2 = 10$, $m = 20$, $r = 1$, $\mathscr{F} = 0$, $\mathscr{S} = 0$. Stable regions are denoted by S, unstable regions by U (—)$\beta = 0$; (- - -)$\beta = 0.1$.

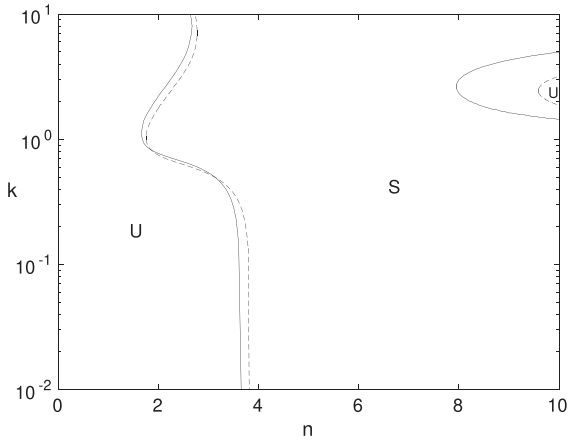

FIG. 13. Neutral stability diagram for the interfacial mode. Flow parameters: $Re_2 = 10$, $m = 20$, $r = 1.5$, $\mathscr{F} = 0.1$, $\mathscr{S} = 0$ Stable regions are denoted by S, unstable regions by U (—)$\beta = 0$; (- - -)$\beta = 0.1$.

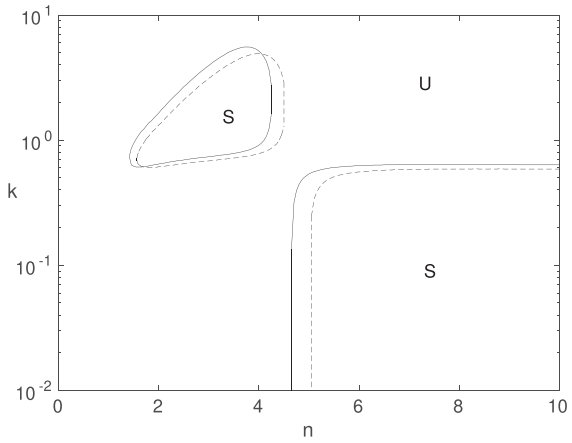

FIG. 14. Effect of slip on a destabilizing density two-layered flow. Flow parameters: $Re_2 = 10$, $m = 20$, $r = 0.5$, $\mathscr{F} = -0.01$, $\mathscr{S} = 0$. Stable regions are denoted by S, unstable regions by U (—)$\beta = 0$; (- - -)$\beta = 0.1$.

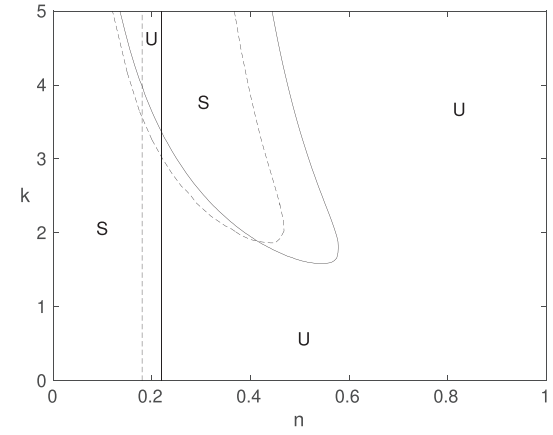

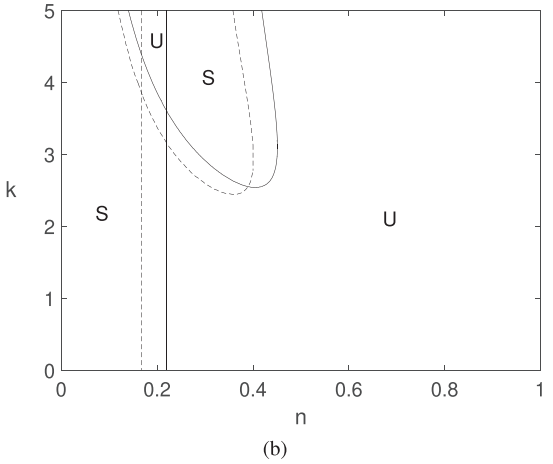

FIG. 15. Neutral stability diagram for the interfacial mode for (a) $Re_2 = 1$ (b) $Re_2 = 10$. Flow parameters: $\mathscr{F} = 0$, $m = 0.05$, $r = 1$, $\mathscr{S} = 0$. Stable regions are denoted by S, unstable regions by U (—)$\beta = 0$; (- - -)$\beta = 0.01$; (-···-)$\beta = 0.02$.

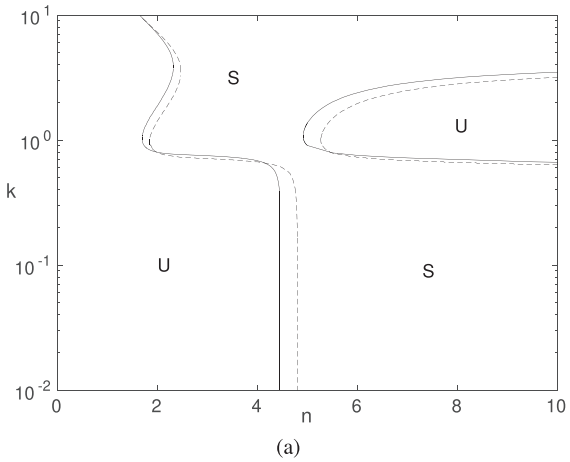

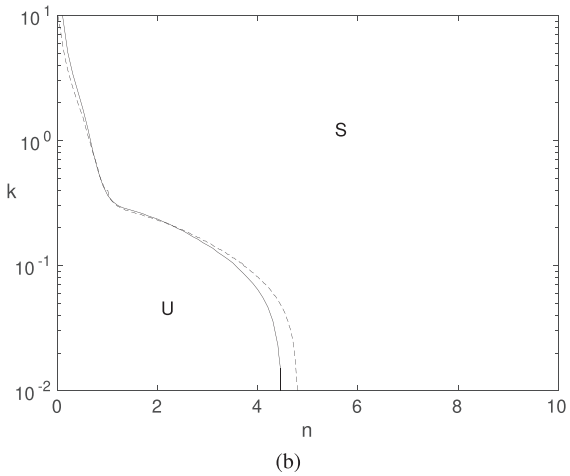

FIG. 16. Neutral stability diagram for the interfacial mode for (a) $\mathscr{S} = 0.01$ (b) $\mathscr{S} = 10$. Flow parameters: $Re_2 = 10$, $m = 20$, $r = 1$. Stable regions are denoted by S, unstable regions by U (—)$\beta = 0$; (- - -)$\beta = 0.1$.

shear and interfacial modes of instability, in the absence of gravity and surface tension effects. This highlights the stabilizing influence of slip on the flow system.

In the case of a flow system with an extremely viscous bottom layer when compared to the top layer ($m = 20$), we observe a destabilizing effect of slip for small wavenumber disturbances ($k < 0.8$), even in the presence of stabilizing interfacial surface tension ($\mathscr{S} > 0$) and gravity effects ($r > 1, \mathscr{F} > 0$). However, for relatively large wavenumber disturbances [$k = O(1)$], the introduction of slip acts as a stabilizing influence on the system, which is observed in the form of a decrease in the unstable regions of flow. When gravity effects are destabilizing ($r < 1, \mathscr{F} < 0$), there is a destabilizing effect on the system upon the introduction of slip.

When the viscosity of the top layer is substantially higher than the bottom layer ($m = 0.05$), we notice that an increase in the slip length β acts as a destabilizing influence on the flow system, as observed by the increase in the unstable regions of flow at the exception of the stable regions. When stabilizing gravity effects are

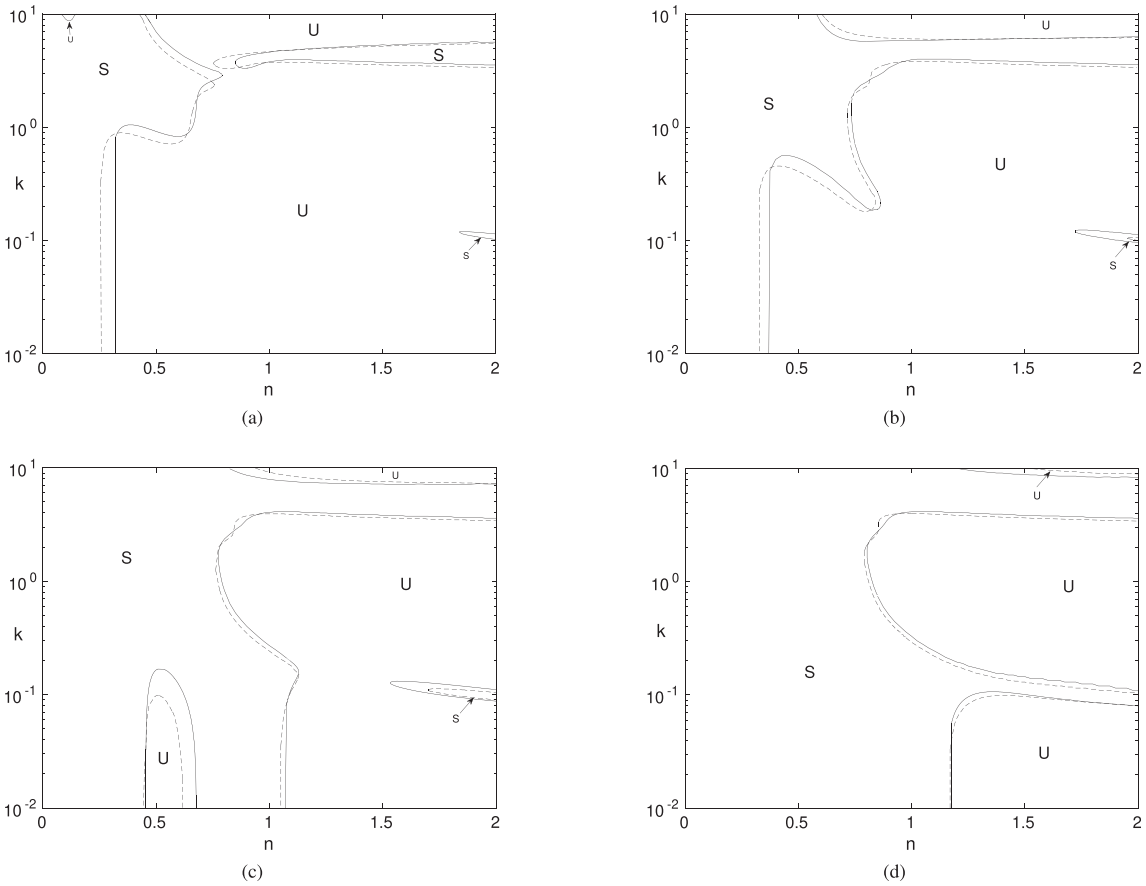

FIG. 17. Neutral stability diagram for the interfacial mode for (a) $\mathscr{F} = 0.6$; (b) $\mathscr{F} = 1$; (c) $\mathscr{F} = 1.5$; (d) $\mathscr{F} = 2$. Flow parameters: $m = 0.05$, $Re_2 = 10$, $\mathscr{S} = 0$, $r = 1.5$. Stable regions are denoted by S, unstable regions by U. (—)$\beta = 0$; (- - -)$\beta = 0.1$.

considered ($r > 1, \mathscr{F} > 0$), the introduction of slip has a predominantly destabilizing effect on the flow system.

SUPPLEMENTARY MATERIAL

See the supplementary material for coefficients given in Eqs. (56) and (69) obtained in zeroth and first order solutions of long-wave analysis.

ACKNOWLEDGMENTS

The authors A. Roy and V. Ramakrishnan acknowledge financial support from IIT Madras initiation Grant No. APM1617836NFIGANUB. The authors would also like to thank H. Mishra for several helpful discussions.

DATA AVAILABILITY

The data that support the findings of this study are available within the article and its supplementary material.

REFERENCES

[1]C.-S. Yih, "Instability due to viscosity stratification," J. Fluid Mech. **27**(2), 337–352 (1967).
[2]A. P. Hooper and W. G. C. Boyd, "Shear-flow instability at the interface between two viscous fluids," J. Fluid Mech. **128**, 507–528 (1983).
[3]S. G. Yiantsios and B. G. Higgins, "Linear stability of plane Poiseuille flow of two superposed fluids," Phys. Fluids **31**(11), 3225–3238 (1988).
[4]F. Charru and J. Fabre, "Long waves at the interface between two viscous fluids," Phys. Fluids **6**(3), 1223–1235 (1994).
[5]B. S. Tilley, S. H. Davis, and S. G. Bankoff, "Linear stability theory of two-layer fluid flow in an inclined channel," Phys. Fluids **6**(12), 3906–3922 (1994).
[6]R. Kushnir, V. Segal, A. Ullmann, and N. Brauner, "Inclined two-layered stratified channel flows: Long wave stability analysis of multiple solution regions," Int. J. Multiphase Flow **62**, 17–29 (2014).
[7]A. Kaffel and A. Riaz, "Eigenspectra and mode coalescence of temporal instability in two-phase channel flow," Phys. Fluids **27**(4), 042101 (2015).
[8]I. Barmak, A. Gelfgat, H. Vitoshkin, A. Ullmann, and N. Brauner, "Stability of stratified two-phase flows in horizontal channels," Phys. Fluids **28**(4), 044101 (2016).
[9]C. L. M. H. Navier, "Mémoire sur les lois du mouvement des fluides," Mém. l'Acad. R. Sci. l'Inst. France **6**, 389–440 (1823).
[10]K. Watanabe and H. Mizunuma, "Slip of Newtonian fluids at slid boundary," JSME Int. J., Ser. B **41**(3), 525–529 (1998).
[11]D. C. Tretheway and C. D. Meinhart, "Apparent fluid slip at hydrophobic microchannel walls," Phys. Fluids **14**(3), L9–L12 (2002).
[12]R. Pit, H. Hervet, and L. Leger, "Direct experimental evidence of slip in hexadecane: Solid interfaces," Phys. Rev. Lett. **85**(5), 980 (2000).

[13]Y. Zhu and S. Granick, "Limits of the hydrodynamic no-slip boundary condition," Phys. Rev. Lett. **88**(10), 106102 (2002).
[14]V. S. Craig, C. Neto, and D. R. Williams, "Shear-dependent boundary slip in an aqueous Newtonian liquid," Phys. Rev. Lett. **87**(5), 054504 (2001).
[15]P. A. Thompson and S. M. Troian, "A general boundary condition for liquid flow at solid surfaces," Nature **389**(6649), 360–362 (1997).
[16]M. Sun and C. Ebner, "Molecular dynamics study of flow at a fluid-wall interface," Phys. Rev. Lett. **69**(24), 3491 (1992).
[17]N. V. Churaev, V. D. Sobolev, and A. N. Somov, "Slippage of liquids over lyophobic solid surfaces," J. Colloid Interface Sci. **97**(2), 574–581 (1984).
[18]O. I. Vinogradova, "Slippage of water over hydrophobic surfaces," Int. J. Miner. Process. **56**(1–4), 31–60 (1999).
[19]Y. Ichikawa, K. Yamamoto, M. Yamamoto, and M. Motosuke, "Near-hydrophobic-surface flow measurement by micro-3D PTV for evaluation of drag reduction," Phys. Fluids **29**(9), 092005 (2017).
[20]R. S. Voronov, D. V. Papavassiliou, and L. L. Lee, "Review of fluid slip over superhydrophobic surfaces and its dependence on the contact angle," Ind. Eng. Chem. Res. **47**(8), 2455–2477 (2008).
[21]B. Liu and Y. Zhang, "A numerical study on the natural transition locations in the flat-plate boundary layers on superhydrophobic surfaces," Phys. Fluids **32**(12), 124103 (2020).
[22]G. S. Beavers and D. D. Joseph, "Boundary conditions at a naturally permeable wall," J. Fluid Mech. **30**(1), 197–207 (1967).
[23]J. M. Gersting, Jr., "Hydrodynamic stability of plane porous slip flow," Phys. Fluids **17**(11), 2126–2127 (1974).
[24]E. Lauga and C. Cossu, "A note on the stability of slip channel flows," Phys. Fluids **17**(8), 088106 (2005).
[25]T. Min and J. Kim, "Effects of hydrophobic surface on stability and transition," Phys. Fluids **17**(10), 108106 (2005).
[26]R. Ling, C. Jian-Guo, and Z. Ke-Qin, "Dual role of wall slip on linear stability of plane Poiseuille flow," Chin. Phys. Lett. **25**(2), 601 (2008).
[27]C. Chai and B. Song, "Stability slip channel flow revisited," Phys. Fluids **31**(8), 084105 (2019).
[28]A. Samanta, "Non-modal stability analysis in viscous fluid flows with slippery walls," Phys. Fluids **32**(6), 064105 (2020).
[29]G. Chattopadhyay and R. Usha, "On the Yih-Marangoni instability of a two-phase plane Poiseuille flow in a hydrophobic channel," Chem. Eng. Sci. **145**, 214–232 (2016).
[30]L. N. Trefethen, *Spectral Methods in MATLAB* (Society for Industrial and Applied Mathematics, 2000).
[31]A. Samanta, C. Ruyer-Quil, and B. Goyeau, "A falling film down a slippery inclined plane," J. Fluid Mech. **684**, 353 (2011).
[32]C.-J. Gan and Z.-N. Wu, "Short-wave instability due to wall slip and numerical observation of wall-slip instability for microchannel flows," J. Fluid Mech. **550**, 289 (2006).
[33]X.-Y. You and J.-R. Zheng, "Stability of liquid-liquid stratified microchannel flow under the effects of boundary slip," Int. J. Chem. Reactor Eng. **7**(1), A85 (2009).
[34]J. P. Pascal, "Linear stability of fluid flow down a porous inclined plane," J. Phys. D: Appl. Phys. **32**(4), 417 (1999).
[35]S. Chakraborty, T. W.-H. Sheu, and S. Ghosh, "Dynamics and stability of a power-law film flowing down a slippery slope," Phys. Fluids **31**(1), 013102 (2019).
[36]A. Ullmann, M. Zamir, Z. Ludmer, and N. Brauner, "Stratified laminar countercurrent flow of two liquid phases in inclined tubes," Int. J. Multiphase Flow **29**(10), 1583–1604 (2003).
[37]D. Lumma, A. Best, A. Gansen, F. Feuillebois, J. O. Rädler, and O. I. Vinogradova, "Flow profile near a wall measured by double-focus fluorescence cross-correlation," Phys. Rev. E **67**, 056313 (2003).
[38]U. C. Boehnke, T. Remmler, H. Motschmann, S. Wurlitzer, J. Hauwede, and M. Th. Fischer, "Partial air wetting on solvophobic surfaces in polar liquids," J. Colloid Interface Sci. **211**, 243–251 (1999).
[39]E. Lauga, M. P. Brenner, and H. A. Stone, "Microfluidics: The no-slip boundary condition," arXiv:cond-mat/0501557 (2005).
[40]K. A. Nair and A. Sameen, "Experimental study of slip flow at the fluid-porous interface in a boundary layer flow," Proc. IUTAM **15**, 293–299 (2015).
[41]K. A. Nair, A. Sameen, and S. A. Lal, "Passive boundary layer flow control using porous lamination," Transp. Porous Media **124**(2), 533–551 (2018).
[42]J. Lu, H. K. Jang, S. B. Lee, and W. R. Hwang, "Characterization on the anisotropic slip for flows over unidirectional fibrous porous media for advanced composites manufacturing," Composites, Part A **100**, 9–19 (2017).